POLITECNICO DI TORINO

Mechatronics Engineering

Master Degree Thesis

Optical fiber thermo-optical coefficient determination for sensing application

Reference teachers
Eugenio BRUSA
Cristiana DELPRETE

Candidate
Théo METEZEAU

POLITECNICO DI TORINO

Mechatronics Engineering

Master Degree Thesis

Optical fiber thermo-optical coefficient determination for sensing application

Reference teachers
Eugenio BRUSA
Cristiana DELPRETE

Candidate
Théo METEZEAU

Acknowledgments

First of all, I would like to thank all the people that helped me during this thesi.

I would like to thank profusely my reference teachers, **professor Eugenio Brusa** and **professor Cristiana Delprete**, professors of the DIMEAS (Department of Mechanical and Aerospace Engineering) for the time they spent for me during this thesi, their confidence and their presence in the delicate and important moments. I also want to thank another teacher, **professor Paolo Maggiore** for giving me access to the laboratory where I got the chance to develop my experimental part.

I would like now to conclude these acknowledgments, thanking three people: **Teo Scolpito**, **Giancarlo Candiano** and **Andrea Coscia**, that are three students of the Politecnico that were also doing a thesi related to fiber optics; for their team spirit, the time they gave me and their precious help every time I needed it.

Abstract

This project, developed within the Polytechnic University of Turin, aimed to develop a test bench with a feedback loop to determine the thermo-optical coefficient of optical fibers used to measure different physical quantities such as elongation, vibrations or even the temperature. These fibers comprise a Bragg grating which enables them to let pass the entire light spectrum passing through them except for a wavelength which is reflected and which depends on the value(s) which is/are to measure. Thus, the test bench developed for this project allows us to precisely vary the temperature of the fiber that we want to study. The response of the fiber is a shift of wavelength of the reflected wave. Since the temperature variation is directly related to the shift of the wavelength of the reflected wave by the thermo-optical coefficient of the optical fiber studied, we obtain the desired result.

Keywords : Optical fiber, Fiber optics, Fiber Bragg Grating, Wavelength shift, Reflected wave, Temperature measurement

Contents

I Introduction

I - 1 Context

The development of structure monitoring (crucial to maintain safety) technics throughout the years enabled to reduce the cost liked to maintenance on infrastructures and to increase their longevity via the early risks detection allowing preventative maintenance. Nowadays, smart technologies, such as fiber Bragg grating (FBG) monitoring, are more and more applied for structure monitoring as they provide real-time evolution of the different parameters of interest such as vibration, strain or even temperature.

I - 2 Objective

The objective of this project, developed within the PhotoNext facilities (photonics pole of the Polytechnic University of Turin), is to create a test bench that we will then be used to determine the thermo-optical coefficient of a sensing optical fiber, the sensing being done via the Bragg grating inside the core of the fiber.

I - 3 Developed system and methodology

The system that has been developed is a test bench provided with a feedback loop, to precisely control the temperature of the fiber undergoing the test to determine its thermo-optical coefficient. Thanks to this controlled test bench, we precisely vary the temperature of the fiber. The response of the fiber is a shift of wavelength of the reflected wave. The temperature variation being directly linked to the reflected wavelength variation with this sensing method by the thermo-optical coefficient of the fiber, we obtain the desired result.

II Presentation of the laboratory

II - 1 The Polytechnic University of Turin

The Polytechnic University of Turin (Politecnico di Torino, in italian), is a public engineering university located in Turin. Founded in 1859, it is actually the oldest technical university of Italy and it proposes courses in three different fields : architecture, engineering and industrial design. The Royal Turin Polytechnic (Regio Politecnico di Torino, in italian) was established in 1906, but the current institution was preceded by the Technical School for Engineers (Scuola di Applicazione per gli Ingegneri, in italian) , which was founded in 1859 and the Italian Industry Museum (Museo Industriale Italiano, in italian) founded in 1862.

The current main complex of buildings, located in Corso Duca degli Abruzzi, was inaugurated in November 1958, with the aim to expand both the volume and the facilities that the Valentino Castle (a House of Savoy of the 17th century), historical headquarters of the school, was offering so far. This expansion continued during the 90s, with the creation in Alessandria, Biella, Ivrea and Mondovì of new teaching campuses.

Nowadays, the Valentino Castle, located on the River Po, is the main architecture teaching campus whereas the building in corso Duca degli Abruzzi together with the Cittadella Politecnica, are the engineering main campuses.

Throughout the years, the Polytechnic University of Turin has become a major university, not only in Italy, but also in Europe and in the world. It counts approximately 33,500 students, with more than 14% of them being international students coming from 120 countries. All this students are offered to choose between 22 different degrees for the bachelor, between 29 for the master and 16 different PhD programs. They also get the opportunity to choose to study in English as 19 educational paths are provided in this language, enlighting the international dimension of this university, that gets 469 international agreements. This university is also very attractive to students with its high employment rate of master's graduates. Actually, one year after their graduation, almost 85% of the graduates are employed, that is nearly 12% above the national average in Italy.

The Polytechnic of Turin is also deeply linked to the industry world providing research, development, consulting and even more to companies such as Microsoft, Ferrari or Bosch for example.

For all this reasons, the Polytechnic of Turin, since its creation 159 years ago, has become a major school on the international level, ranked in the top 50 of the 2018 QS World University Ranking in architecture and engineering and awarded of certifications such as the « HR Excellence in Research » by the European Commission.

II - 2 The PhotoNext

The traffic of data is about to experience a tremendous growth in the coming years due to various factors like the augmented-reality contents or the access to the 5G for example. To answer to these (future) demands and problems, the data networks based on optical signals, backbone of the internet revolution, are the current solutions. A clear example of the contribution of this technology in our daily life is the access to ultra-broadband when the copper telephone network was substituted with the optical fibers network.

Despite the current technology performances, it is necessary to improve the currently available technology to face the coming challenges and needs of the society and industry.

In order to be an active actor in this process, the Polytechnic of Turin, that is seen as a research university, created, in 2017, a multidisciplinary center of competence on photonics (technology based on optical signals) : the PhotoNext center. With a budget of 1.8M€ for the three coming years, it aims to become one of the best centers in the world in experimental capabilities on photonics. The areas covered by this center are the creation/development of optical components with novel features, the creation of brand-new sensors for daily life and safety and, finally, the development ultra-high speed networks for optical communications.

The Polytechnic University of Turin, via the PhotoNext center, also wants to extend its mastery about this technology and to provide new solutions to other fields than telecommunication and industry, such as system monitoring with application in aerospace, automotive or even the monitoring of structures, based on this technology using for example the multiple sensing capabilities that it provides.

The link of this university with the industry is also present in this center as the PhotoNext intends to assist, provide consulting and access to the facilities to companies willing to prosper, take advantages, of the industry 4.0.

III Theoretical part

III - 1 Introduction to fiber Bragg grating sensors (FBG)

This technology, that was demonstrated in 1978 by the physicist Dr. Kenneth O. Hill, was originally developed for fiber-optic communications, where it can be used for filters or wavelength multiplexers, for example. Very quickly, this technology has been the subject of developments for sensing applications, because of the capacity of the optical fiber to be able to serve as both a sensitive and transmission element (in the case of intrinsic optical sensors). Among all the sensors based on the use of optical fiber, FBG sensors are among the most used.

Fundamentally, an optical fiber sensor modulates one or more properties of the transmitted light wave, including its intensity, phase, polarization or frequency, in response to the measured environmental parameter. In the case of an FBG sensor, it reflects a wavelength of light that fluctuates as a function of temperature and/or strain variations.

These sensors, exploited in reflection, are convenient to realize a serialization of the sensing segment (FBG), by shifting the wavelength ranges of the different FBGs, and interrogating them by reflectometry. This produces a distributed sensor that can combine several tens of elementary sensors along a single fiber. Their main interest is their ease of integration along the fiber, as well as their high reading rate (several kHz). They are very used for the surveillance of nuclear and aeronautical structures or even historical monuments thanks to their minimally invasive character.

III - 2 Fiber Bragg grating sensing principle

While conventional optical fiber interferometric sensors need as a light source a highly coherent lasers, FBG sensors require a light source that is broadband and a wavelength-shift detection system with a high resolution. The light source needs to get a wide wavelength bandwidth and a high optical power in order to obtain a large range of inspection together with a good resolution to see precisely the wavelength shift induced by the measurand.

When a broad spectrum light beam is sent to an FBG, the reflections emitted by each alternating refractive index segment interfere constructively only for a particular wavelength that is called the Bragg wavelength. As a result, the FBG only reflects the specific wavelength, the Bragg wavelength, and transmits all the others wavelengths as we can see in Fig.1 .

The Bragg wavelength λ_B is linked to the effective core index of refraction n and to the grating pitch Λ by the following formula, formula 1 :

$$\lambda_B = 2.n.\Lambda \tag{1}$$

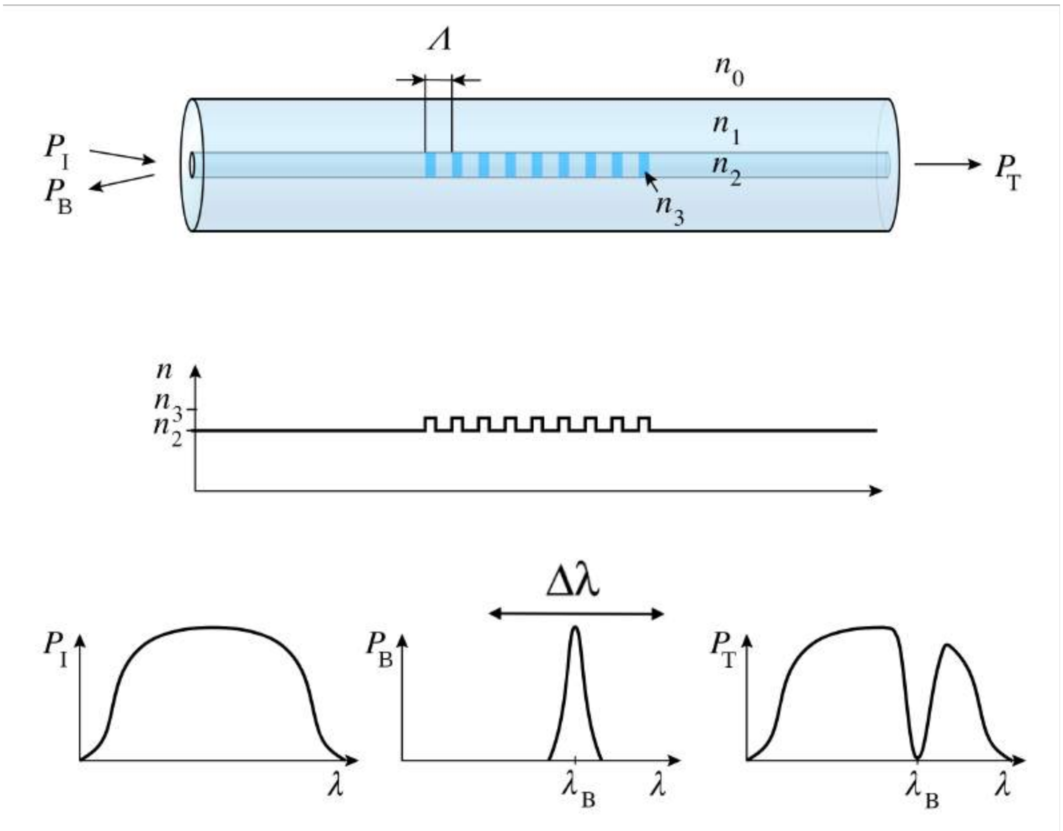

Figure 1: Fiber Bragg grating sensing principle,
Matthias Krüger, Fiber Bragg Grating, 2008

Strain and temperature variations affect both the effective refractive index n and the grating pitch Λ of the FBG, which results in a shift of the reflected wavelength. The reflected wavelength shift of a FBG due to strain and temperature changes can be described by the following formula, formula 2 ; where $\Delta\lambda_B$ is the shift of the wavelength, λ_B the initial wavelength, where p_e is the optical stress coefficient and ϵ is the stress experienced by the grating, where α_Λ is the thermal expansion coefficient, α_n the thermo-optical coefficient and ΔT the variation of temperature.

$$\Delta\lambda_B \;=\; [\;(1\;-\;p_e).\epsilon\;+\;(\alpha_\Lambda\;+\;\alpha_n).\Delta T\;].\lambda_B \tag{2}$$

α_n describes the variation of the refractive index while α_Λ describes the expansion of the network, both due to the temperature. The coefficient of expansion α_Λ of the glass being almost negligible, the reflected wavelength shift due to the temperature variation can be described by the variation of the refractive index α_n of the fiber.

III - 3 Fabrication processes of FBG

III - 3 - 1 Inscription of the Bragg grating

In order to write the Bragg grating within the core of the optical fiber, the process is the following : we expose to a periodic distribution of light intensity a section of photosensitive fiber. This exposition modify permanently the refractive index of the fiber. Usually, optical fibers are doped with germanium (Ge-doped). The result of that doping is an augmentation of the refractive index that makes the fiber ultraviolet (UV) photosensitive (the amount of refractive index change depends on three parameters

: the exposure duration and intensity as well as the photosensitivity of the fiber). This means that an exposition to UV light generate a refractive-index change that is permanent. It is also possible to enhance the photosensitivity of the fibers (such as the one used for telecommunication networks that do not have a Ge-doped core) via various techniques. First, there is the hydrogen loading technique, where the photosensitivity of the fiber is enhanced via an hydrogen pre-soaking. Another technique is the flame brushing where the fiber is brushed, with a hydrogen fueled flame at a temperature 1700˚C. This technique has the advantage not to modify the properties of the cladding, and compare to the previous hydrogen process, the enhancement of the photosensitivity is permanent. Nonetheless, the fiber, because of the exposure to a flame, is then more fragile. The last method is to co-dope (the fiber is already Ge-doped) the fiber with another dopant such as boron or erbium for example.

There are several methods to produce gratings in photosensitive optical fibers and we now described them.

III - 3 - 2 Two-beam interferometer technique

This category includes 2 differents techniques [17]. The first technique, the holographic method, is based on two-beam interference. in this method, a UV laser sourve is divided into two different beams that then interfere with each other (after reflection on mirrors) generating, along the interference pattern, a periodic intensity distribution as we can see in Fig.2. As the fiber refractive index is modified proportionally to light intensity it is exposed to, the Bragg grating is written inside the fiber core. The main advantage of this technique, that explains that is was the first to be widely used to produce fiber Bragg gratings, is that it is easily tunable as the Bragg wavelength is a function of the laser incident angle. A modification of the angle would modify the interference period and thus the Bragg grating as we can see in the formula 3 where Λ is the Bragg grating pitch, λ_{UV} the wavelength of the UV light source and φ the angle between the writing beam and the fiber normal axis.

$$\Lambda = \lambda_{UV} / \varphi \tag{3}$$

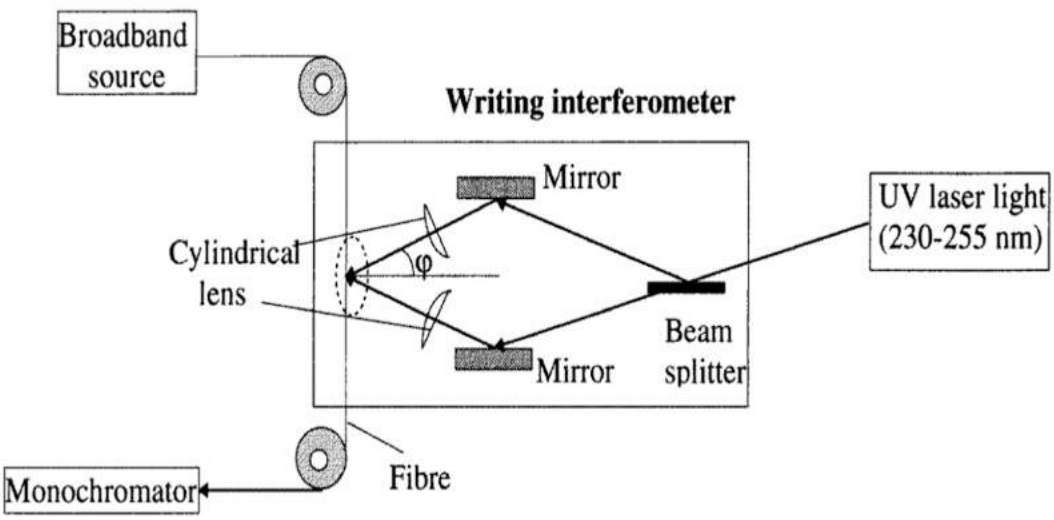

Figure 2: Two-beam interferometer technique, ref.17

The second technique is called source-tunable interferometer method. This method is solving, overcoming the disadvantages of the previously presented process. The source-tunable interferometer process permits to select the Bragg wavelength by tuning the UV light source wavelength instead of the angles of the mirrors [17]. Here the variation of angles of the two mirrors is used to extend the FBG wavelength range. The Bragg wavelengths that are obtainable with this technique are given by the formula 4 :

$$\lambda_B = \frac{n.\lambda_{UV}}{sin(\theta_p + 2\theta_m)} \tag{4}$$

with n the effective core index of refraction, λ_B the Bragg wavelength, λ_{UV} the wavelength of the UV light source, θ_p the angle between the writing beam and the fiber normal axis, and θ_m the mirror angle. Fig.3 shows the source-tunable interferometer method.

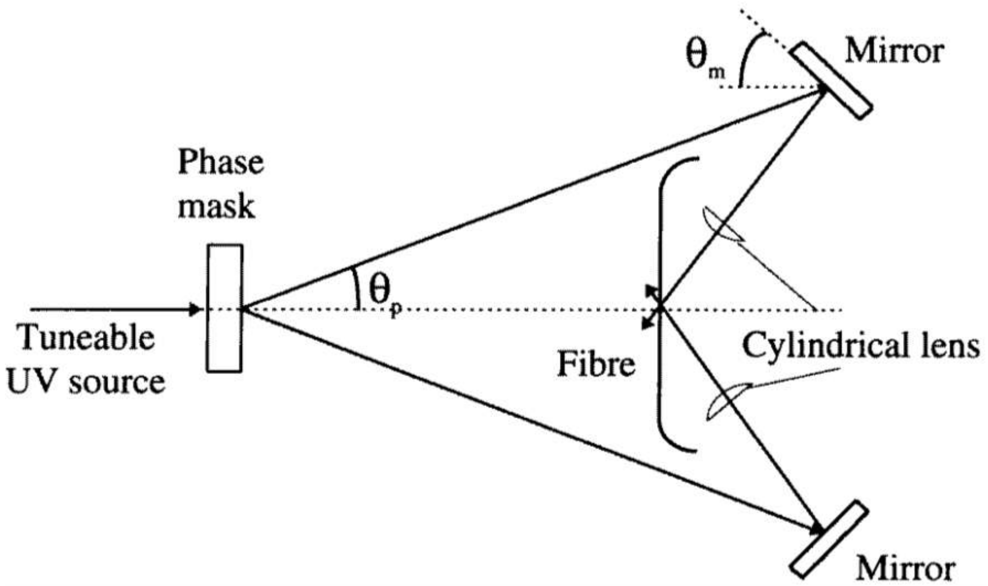

Figure 3: Source-tunable interferometer technique, ref.17

III - 3 - 3 Phase-mask technique

The principle of this method, nonholographic, that is widely used nowadays consists in placing a diffractive element between the UV light source and the fiber. The element called a mask is placed near and in parallel of the fiber in order to create, with the UV beam of the light source that is diffracted when passing the mask, an interference pattern that will photo-imprint, inside the core of the fiber, the refractive index modulation that will generate the Bragg grating [17] as we can see in Fig.4.

This process presents several advantages compared to the two-beam interferometer process. First, the Bragg wavelength of the written Bragg grating inside the fiber core is independent of the UV laser wavelength and is given by the phase-mask pitch. Then, it offers the possibility of mass production at relatively low cost with a great repeatability as the mask used for this method are made by computer-controlled photolithographic imprinting process. Another advantage of the phase-mask technique is that, unlike the two-beam interferometer, the UV laser source do not have to be highly coherent, thus it reduces the cost of fabrication.

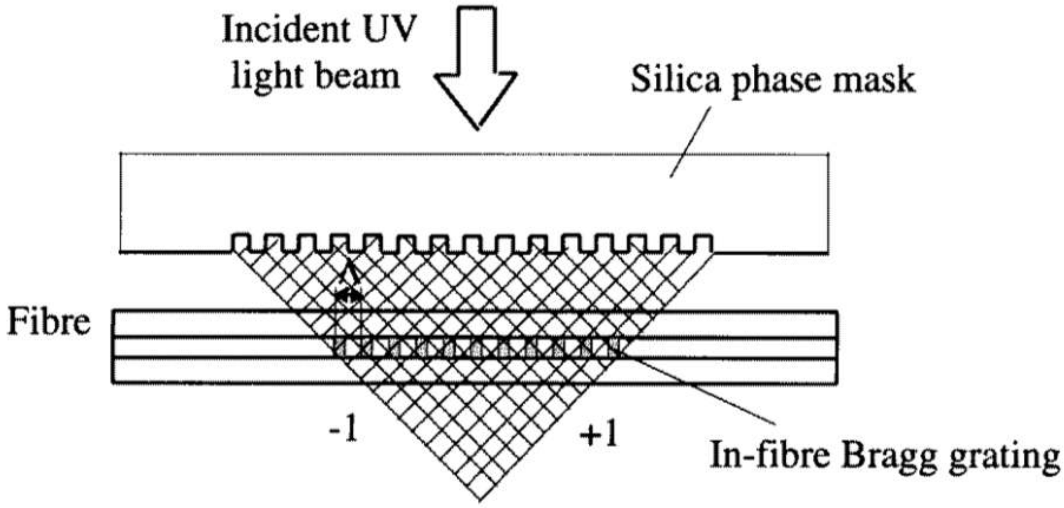

Figure 4: Phase-mask technique, ref.17

It is also important to mention the fact that the phase-mask technique allows the writing of some gratings that can't be written using an interference pattern such as chirped gratings (we will develop later the types of gratings).

This technique has been modified with the use of an incident converging or diverging wavefront on the mask (considering the initial wavefront to be a plane one) in order to modify the Bragg wavelength using a phase-mask that is fixed as we can see in Fig.5.

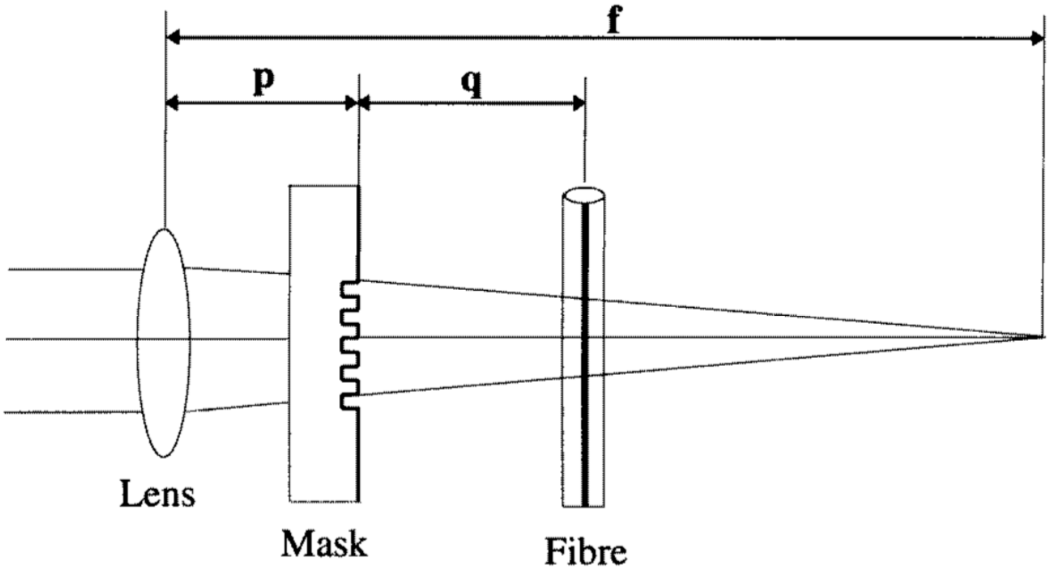

Figure 5: Modified phase-mask method using a lens, ref.17

Using this method, the fiber grating pitch, Λ is linked to the phase-mask pitch d and to the demagnification factor M by the following formula, formula 5 :

$$\Lambda = M.d \tag{5}$$

The demagnification factor M is linked to the focal length f of the lens used to create the incident converging or diverging wavefront, to p that is the distance between the lens and the mask and to the distance between the mask and the fiber q by the formula 6 :

$$M = \frac{f - p - q}{f - p} \tag{6}$$

From the formulas 5 and 6 the advantage of this method is clear : we can tune, varying q or/and p, the grating pitch of the fiber Bragg grating. q being limited because of the UV laser coherence length, the limitation/drawback of this method is the relatively narrow range of tuning (only few tens of nanometers).

Another method, based on the movement of the fiber or/and the mask and called moving fibre/phase-mask scanning, permits, with the use of one mask only, to write FBG with different Bragg wavelengths. The difference compared to the previous process is that the fiber is not fixed relatively to the phase-mask, it moves relatively to it whereas the UV source is printing the grating inside the fiber core.

The last method to produce FBG is called point-by-point. The Bragg grating is written point-by-point via a single UV laser light ray which width equals the period of the grating. This technique is applicable to write tilted or long period gratings. Fig.6 illustrates this process.

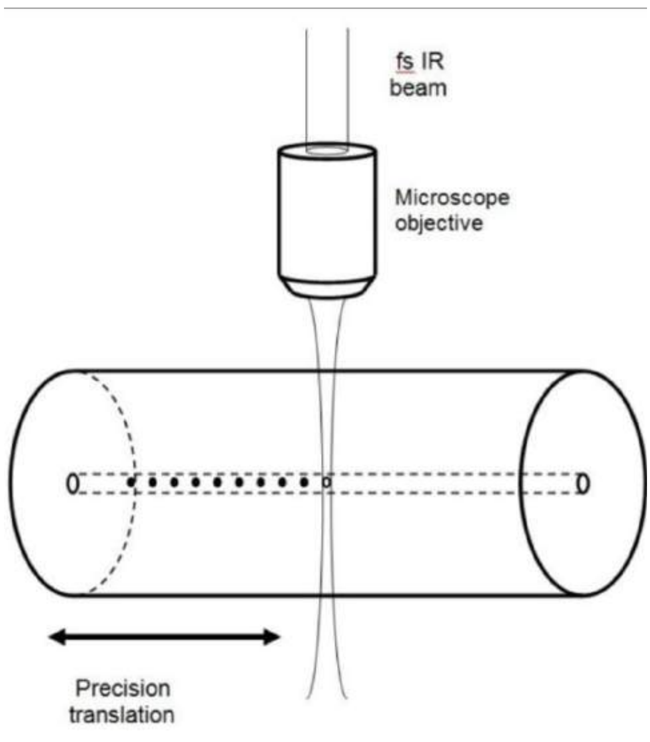

Figure 6: Point-by-point process, ref.14

III - 4 Different types of grating

According to the photosensitivity mechanism that generates the Bragg grating inside the fiber we can distinguish different types of grating. The different processes to generate the gratings have an important impact on the physical capacities of the generated grating such has the high temperature withstanding capability.

III - 4 - 1 Type I gratings

The first type of grating to be presented is the one named type I grating, seen as the standard grating type, has a positive refractive index change. The process to create these gratings is based on a single UV photon absorption that stimulates the ODC (oxygen deficiency defect centers). A densification of the glass matrix is needed in order to obtain a large change of index [14]. The transmission and reflection spectra are complementary.

The problem of the gratings of this type is that they are annealed when the temperature exceeds their designed operating temperature. This means that this type of grating is not suitable for environment where the temperature is above 450˚C [14].

III - 4 - 2 Type II gratings

This second type of gratings, also referred as damage gratings, can be used at temperature over 1.000˚C as they remain stable over this temperature. They are produced with the use of high peak power pulsed UV laser as light source and are written via a single pulse of the laser. The process to create such gratings is based on a threshold dependent multi-photon ionization method.

The drawback of these gratings is that, due to their fabrication process, their mechanical strength and reliability are reduced.

III - 4 - 3 Type In gratings

These kind of gratings, that can be stable and thus used above 700˚C, are written inside the core of Ge-doped fibers that are importantly stressed and get a negative change of refractive index. These gratings were formerly called IIA gratings.

III - 4 - 4 Regenerated gratings

This other type of gratings is made according to the following process : after hydrogen loading to enhance the reflectivity of the fiber, a type I grating structure is written by laser inscription. After that the grating, of type I, that was obtained is annealed at temperature between 600˚C and 700˚C. Then, a new grating is generated by another heating at a more elevated temperature. This new grating has a longer Bragg wavelength than the type I obtained right after the laser inscription and is stable at higher temperatures but, the index modulation of the final structure is lower than the one of the type I.

III - 4 - 5 Femtosecond pulse duration infrared laser induced gratings

These gratings are generated using ultrahigh peak power radiation generated by femtosecond pulse duration infrared (fs-IR) laser [14]. The process of writing, that can be done via the phase-mask or point-by-point technique, is for this type of gratings based on a multi-photon ionization/absorption. Above the ionization threshold intensity, the multi-photon ionization takes place. Material compaction, formation of void and localized melting are the results of this ionization and they are responsible of the change of index with similar attributes than a type II grating generated by nanosecond pulse duration ultraviolet laser. Nonetheless, the gratings developed in this paragraph have, compare to their UV equivalents, better spectral performances.

The first advantage of this process to write gratings is that it permits the grating fabrication in all transparent to the low signal infrared radiation waveguides, and not only in silica UV-photosensitive ones. The second advantage of this process is that it provides thermally stable structures above 1.000˚C for silica based waveguides and even above 1.750˚C for sapphire ones.

III - 5 Different structures of grating

The FBG structure can be tuned varying two parameters : the index of refraction or the period of the grating. The profile of the refractive index can be of two types : uniform or apodized, and the period of the grating can be uniform or not. We are now going to present the more common types of grating.

III - 5 - 1 Uniform gratings

An uniform grating is a grating with a uniform pitch distribution and the grating is perpendicular to the fiber axis as we can see in Fig.7. For this kind of gratings, the profile of the refractive index is given by the following formula, formula 7:

$$n \; = \; n_0 \; + \; \Delta n(z).\cos(\frac{2\pi}{\Lambda}.z \;) \tag{7}$$

with n the effective core index of refraction, n_0 the core index of refraction, $\Delta n(z)$ is the induced refractive index perturbation amplitude, Λ the grating pitch and z along the longitudinal axis of the waveguide. In this case the Bragg wavelength is given by formula 1.

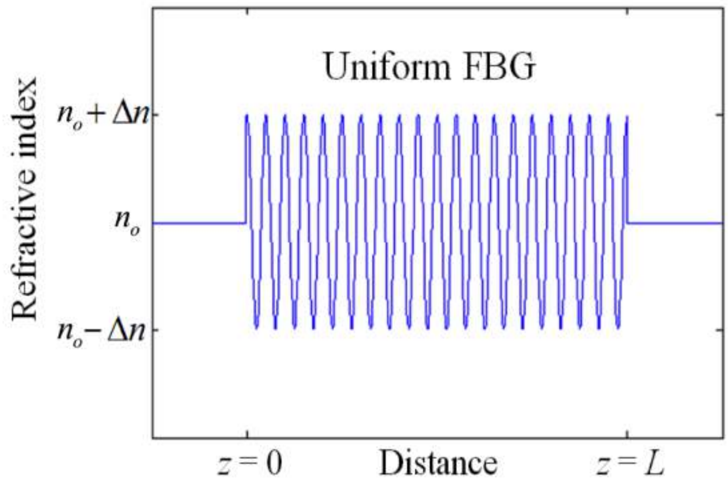

Figure 7: Change of refractive index along uniform FBG, ref.24

III - 5 - 2 Apodized gratings

When using an uniform refractive index modulation, i.e an uniform grating, the main peak of reflection (corresponding to the Bragg wavelength), is accompanied by sidelobes in the reflection spectrum. It is often important or needed (in the case of multiplexing for example) to reduce or even suppress these sidelobes to ensure the proper FBG sensor functionality. To do so, we use an apodized grating.

The so called apodization consists in smoothing the change of refractive inside the core of the fiber at both ends of the grating [12], i.e the change of refractive index is progressive instead of sharp with $\Delta n(z)$ that varies proportionnally to z. Nonetheless this process, despite suppressing the sidelobes decreases, compared to the uniform grating, the maximum reflectivity. The main apodization profiles are : sine, sinc, Gaussian, Hamming, Tanh, Bartlett, Blackman, Cauchy and raised sine.

Fig.8 and 9 compare the apodized structure to the uniform one and the spectrums that result of these two configurations. From Fig.?? the sidelobes suppression is clear.

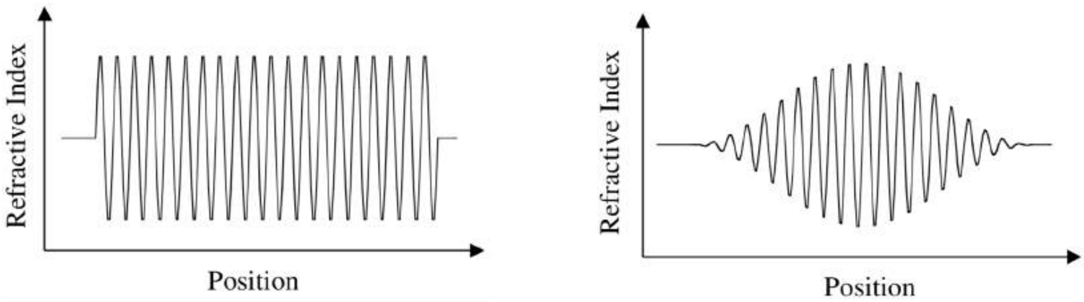

Figure 8: Uniform Bragg grating on the left and apodized grating on the right, ref.19

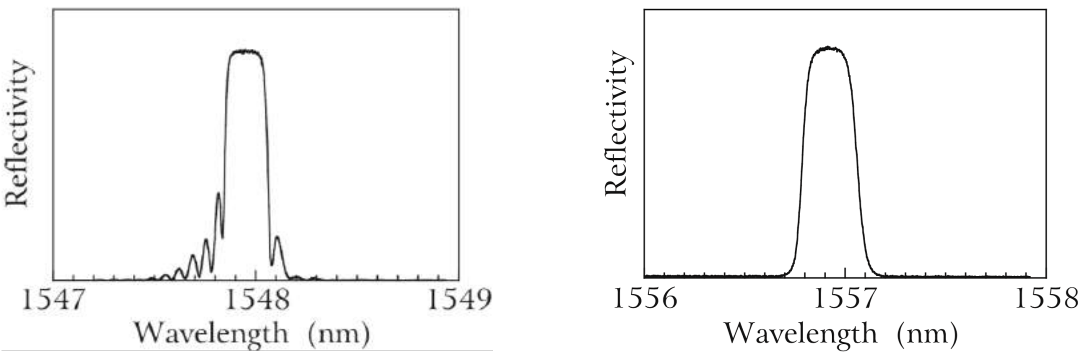

Figure 9: Spectrum from uniform grating with side lobes (left) and spectrum from an apodized grating cancelling side lobes (right), ref.19

The Blackman apodization is the best to reduce the level of the sidelobes. Furthemore we can tune the parameters in order to enhance the different apodizations properties like for example increasing the reflectivity of a type of apodization to be equal to the one of a uniform grating that is the maximum one [23].

III - 5 - 3 Chirped fiber Bragg gratings

Chirped fiber Bragg gratings are characterized by a refractive index modulation that is non-uniform, called a chirp. The modulation periodicity is not constant, it changes along the waveguide axis, z, so that the pitch of the grating is a function of the distance z : Λ(z), as we can see in Fig.10. So, each section of the structure reflects a different Bragg wavelength, and the spetrum of a chirped fiber Bragg gratings is finally given by the spectrum of each section of the grating. The main feature of such gratings is the possibility to interpret temperature and/or strain profiles instead of spatially constant values of these parameters.

For a linearly chirped grating, the Bragg wavelength of reference is linearly varying along the z axis on the length of the grating L according to formula 8 :

$$\lambda_B(z) = \lambda_B(0) + \zeta.z\ ,\ for\ 0 \leq z \leq L \tag{8}$$

where ζ, the chirp rate coefficient, that defines the Bragg wavelength spatial change rate, is constant in a linear chirped fiber Bragg gratings. This type of gratings is between 3 and 10 times longer than an uniform grating (that is around 5mm long) [20].

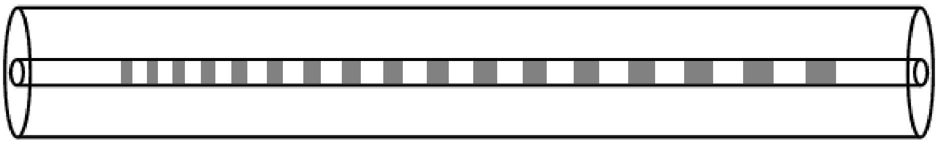

Figure 10: Chirped fiber Bragg gratings

III - 5 - 4 Tilted fiber Bragg gratings

This fourth type of grating, differs from the other types of grating as the grating plane is angled, with respect to the cross section of the fiber, of an angle, the tilt angle ξ. The presence of this angle generates new interesting characteristics. This angle lessens the coupling to the backward core mode, improves the light from the forward-propagating core mode coupling to backward propagating cladding ones and leads to the complex mode coupling occurence. For this grating structure, the Bragg wavelength, λ_B, and the resonance wavelength of the cladding mode, $\lambda_{coupling}$ are given by the following formulas, fomula 9 and 10 :

$$\lambda_B(z) = \frac{2.n_{co,eff}.\Lambda}{\cos(\xi)} \tag{9}$$

$$\lambda_{coupling,i}(z) = \frac{(n_{co,eff} + n_{cladding,i,eff}).\Lambda}{\cos(\xi)} \tag{10}$$

With ξ the tilt angle, $n_{cladding,i,eff}$ the ith cladding mode effective refractive index, $n_{co,eff}$ the core mode effective refractive index. The nominal grating period, Λ, is in this case given by formula 11 where Λ_g is the grating period along the fiber axis.

$$\Lambda = \Lambda_g.\cos(\xi) \tag{11}$$

Fig.11 illustrates the tilted fiber Bragg gratings structure and shows the parameters of interest that we just presented.

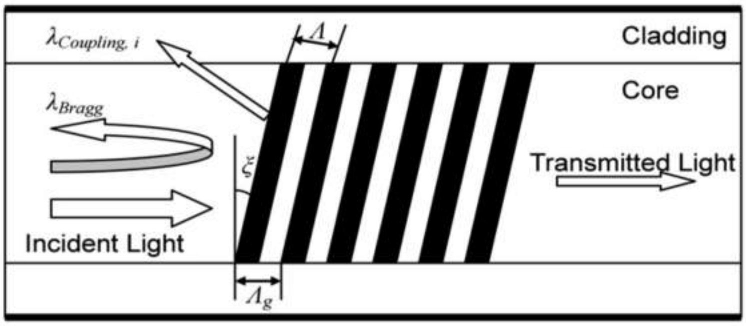

Figure 11: Tilted fiber Bragg gratings, ref.21

III - 5 - 5 Long-period gratings

Long-period gratings are formed by a periodic modulation of the optical fiber properties with a pitch around 100m. This type of grating is highly sensitive to medium surrounding the bare cladding change of index, making it a sensor of the surrounding medium refractive index. The transmission spectrum of such a grating is composed of a number of attenuation bands at resonance wavelengths, each corresponding to the coupling between a co-propagating cladding mode and the guided core mode. On Fig.12 we can see the different modes. The phase-matching equation, formula 12, gives the wavelength at which can be obtained the coupling between the guided mode with the cladding modes.

$$\lambda_m \ = \ (n_{eff}^{co} - n_{eff,m}^{cl}).\Lambda \tag{12}$$

with λ_m the resonance wavelength related to coupling to the m^{th} cladding mode, n_{eff}^{co} the fundamental core mode effective index, $n_{eff,m}^{cl}$ the m^{th} order cladding mode effective index and finally Λ the grating period.

The long-period grating (LPG) resonance wavelength is, as the other gratings, a function of temperature and strain but also of the surrounding refractive index as mentionned earlier. The formula 13 expresses the link between the resonance wavelengths and these three parameters :

$$\Delta\lambda_m \ = \ \frac{d\lambda_m}{dT}.\Delta T \ + \ \frac{d\lambda_m}{d\epsilon}.\Delta\epsilon \ + \ \frac{d\lambda_m}{dn_{sur}}.\Delta n_{sur} \tag{13}$$

with $\frac{d\lambda_m}{d\epsilon}$, $\frac{d\lambda_m}{dT}$ and $\frac{d\lambda_m}{dn_{sur}}$ being respectively the strain, temperature and surrounding refractive index sensitivity.

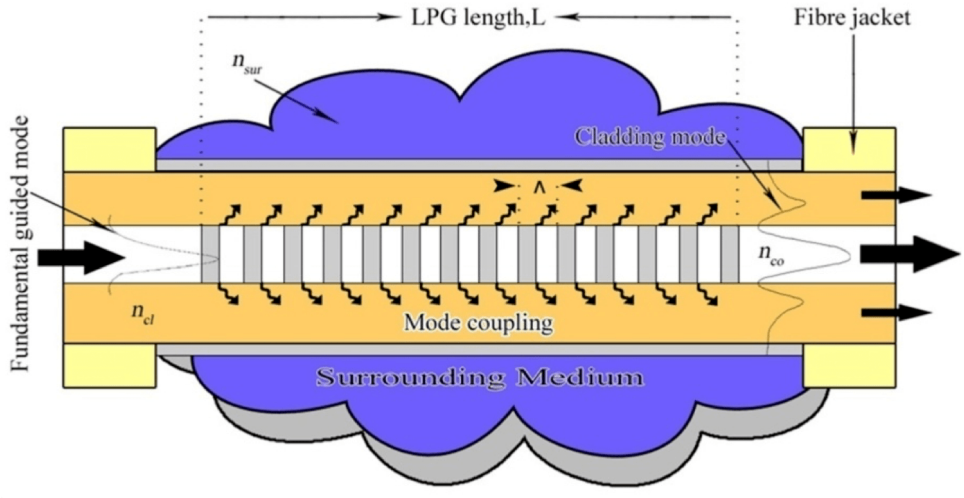

Figure 12: Mode coupling inside a LPG

III - 5 - 6 Phase-Shifted fiber Bragg gratings

Phase-Shifted Fiber Bragg Gratings (PS-FBGs) have special filtering characteristics. Fig.13 illustrates this grating structure (with a π phase). They are made up by two sub-FBGs with phase difference between them, a phase shift. The reflections from the first grating part will destructively interfere with the ones generated by the second grating part as they will be out of phase. This way, an ultra-narrow transmission window is generated, as we can see on Fig.14 where we can see the spectrum of such a grating structure. In order to adapt, tune, the grating according to the situation, we can change, adjusting the phase shift amount, the transmitted wavelength. This configuration is, as the transmission window is ultra-narrow, often used as a demultiplexer.

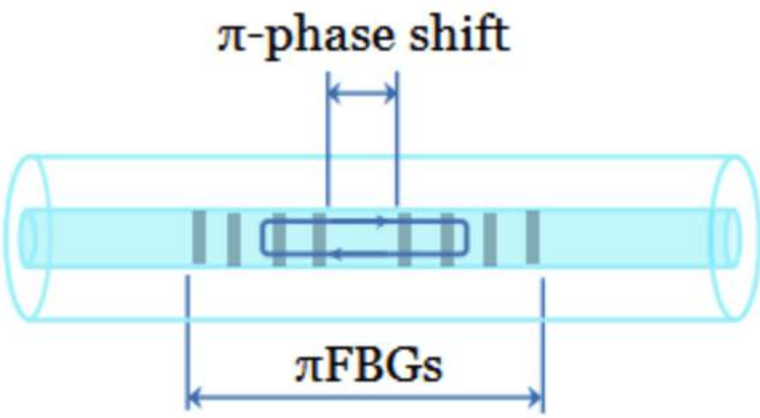

Figure 13: Phase-Shifted fiber Bragg gratings, ref.26

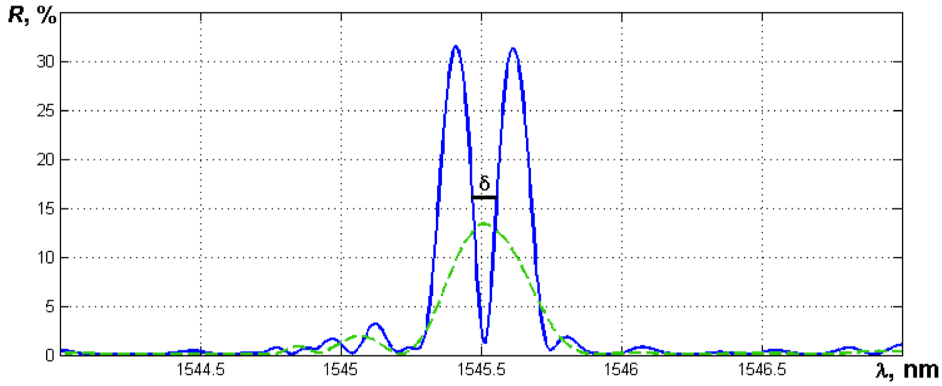

Figure 14: Phase-Shifted fiber Bragg gratings spectrum, ref.26

III - 6 Optical fiber measurement advantages

Optical fiber measurement, using light rather than electricity and optical fibers rather than copper cables, is ideal for applications in which conventional electrical sensors have proven to be ineffective or in harsh environmental conditions such as nuclear power plants.

The ability to write FBGs with unique Bragg wavelengths lends itself well to multiplexing techniques, allowing multiple sensors with different Bragg wavelengths to be cascaded together for a single fiber, reducing considerably the size, weight and complexity of the measuring system.

Moreover, thanks to their lightness and small dimensions, they can be easily implemented on any type of system or building. It should also be noticed that thanks to the lightness of the optical fibers, the FBG sensors do not disturb the measurements (whereas conventional sensors can affect measurements, because of their weight, of vibrations of small systems for example).

Sensors based on this technology also provide a significant advantage from a safety point of view. Indeed, in addition to operating reliably in highly disturbed environments thanks to their insensitivity to electromagnetic interferences, the optical fiber is not conductive. This means that even in the event of malfunction, the fiber can not carry electric currents, which proves to be a major asset in the industrial sector for example.

Finally, the wavelength of the reflected light, unlike its intensity or its polarization, is not modified by its propagation on the optical fiber, which makes it possible to measure the wavelength shift at a distance with perfect fidelity.

III - 7 Application examples

Fiber Bragg grating sensors, thank's to their numerous advantages, are used for a lot of different applications, for temperature monitoring during the fabrication of parts, in aeronautic, for the monitoring of historical monuments or even in medicine. In this section we present some application examples of this technology.

III - 7 - 1 Structure health monitoring

As mentionned earlier in this document, FBG sensing technology is nowadays used in structure health monitoring. It can be used for several reasons such as crack propagation monitoring or to reduce the cost liked to maintenance on infrastructures and to increase their longevity via the early risks detection allowing preventative maintenance.

III - 7 - 2 Airplanes

FBG sensors are also used in the aeronautics domain being embedded on airplanes to monitor the integrity of the plane structure (monitoring the pressure, the deformation, ...). Fig.15 illustrates a possible placement of the fibers to monitor the whole plane structure.

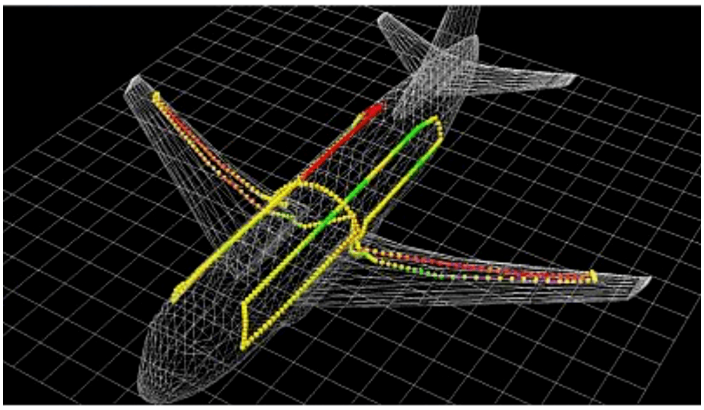

Figure 15: Possible sensing map of a plane using FBG sensing, ref.30

III - 7 - 3 Medical applications

This sensing technology can also be used to medical purposes. It allows to monitor both *in vivo* and *in vitro* [29]. FBG sensing allows to monitor different parts of the body such as : the bones (to understand diseases liked to bones and to study their deformation while they are loaded for example during running or pressing), the joints (to map the pressure inside the articulation and the stresses inside them) or even the chest (to monitor its deformation due to the respiration). It is also used for rehabilitation purposes in order to improve the confort of amputee sockets analysing the pressure distribution. Fig.17, 18 and 16 illustrates how FBG is placed to monitor the chest, bones and joints respectively.

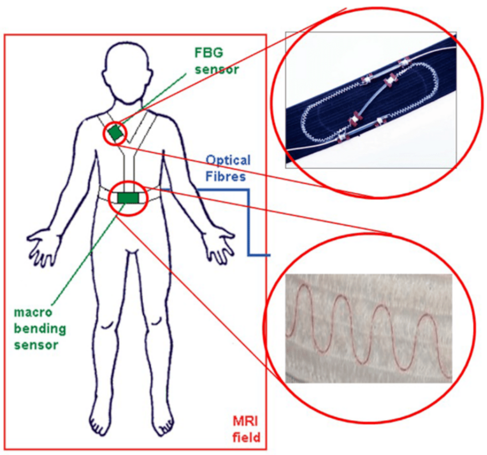

Figure 16: FBG sensing mount for chest deformation monitoring, ref.29

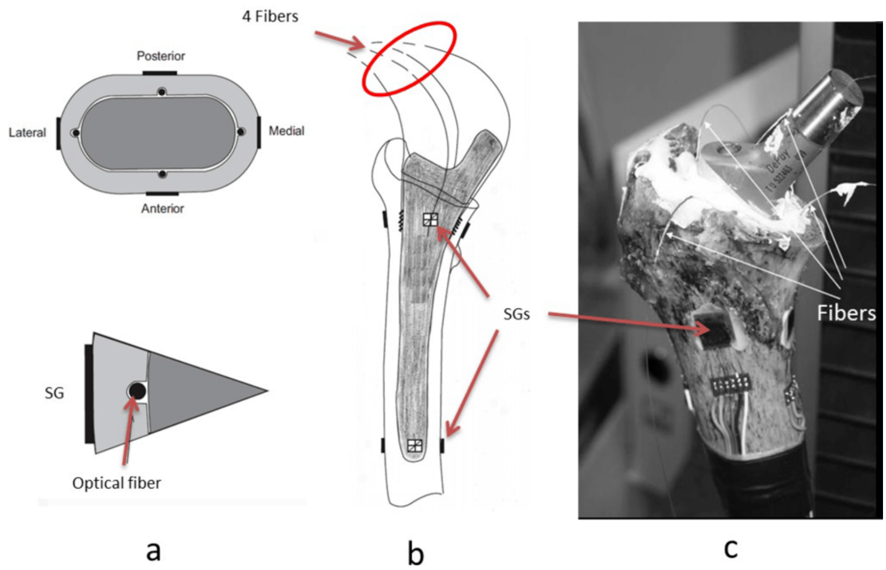

Figure 17: FBG sensing mount for bones monitoring, ref.29

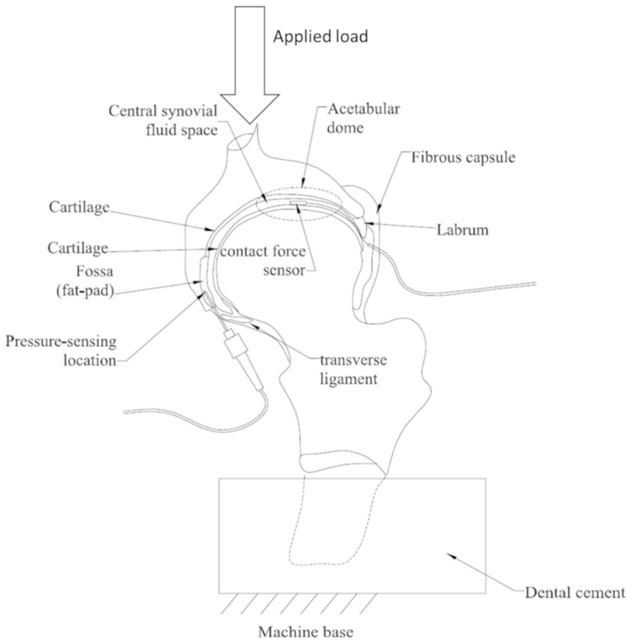

Figure 18: FBG sensing mount for joints monitoring, ref.29

IV Experimental part

IV - 1 Introduction

In this part, we will determine the thermo-optical coefficient of a sensing optical fiber, using the thermal sensing offered by its fiber Bragg grating. As we saw before in the theoretical part, strain and temperature are linked with this sensing technique. Thus, our test bench has to include a strain compensation in order to compensate the possible effects of a strain variation on our measurements.

IV - 2 The test bench

The aim of the test bench is to provide the thermo-optical coefficient of the fiber. In order to do this in the more convenient way possible, we design a system that, once provided the desired temperature, reaches it and remains at this given temperature automatically.

To do so, our system will work according to the following principle: once defined the desired temperature, a controller senses the current temperature of the object thanks to a thermal sensor, compares it to the reference temperature given by the user and thus decides to turn on or off the heating/cooling device (in our case a peltier cell) to reach the previously set temperature.

To this aim, the hardware part of the controlled heating system is composed of: a controller, the TEC 1091, a thermal sensor, the RS Pro PT100 (of class A) and a heating/cooling device, a peltier cell as we said in the previous paragraph, from RS compoments with a power of 5.1W. To control our controller, we use the software TEC Service Sofware V3.00. It allows us to set the desired temperature, displays in real time the temperature of the object undergoing the test (in our case the fiber, see Fig.52 in annexe to see the real time display), and is easily tunable to make the system faster via the PID control included (see Fig.51 in annexe for more details about the setting of the PID).

In the Fig. 19 we can see the setup we use to control the temperature of the test bench, with the controller linked to the sensor, the peltier cell and connected to an alimentation.

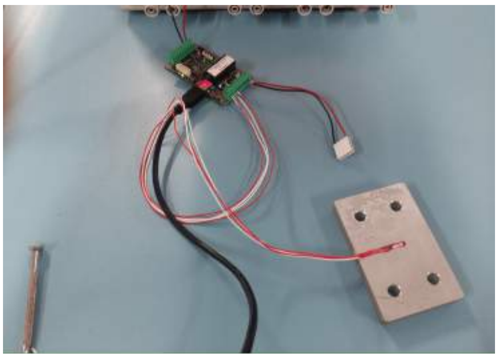

(a) View 1

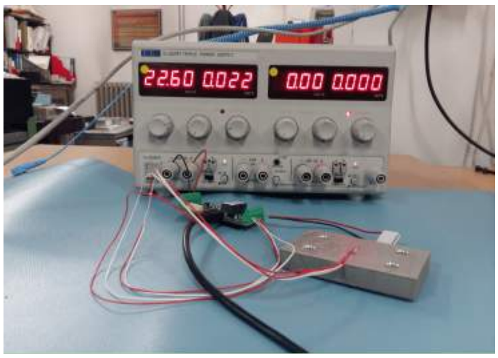

(b) View 2

Figure 19: Different views of the control setup

Then, the controlled heating/cooling and sensing system being done, we design a mounting setup for the fiber that will be tested. In order to compensate the strain variation thus sensing only the temperature variation effects on the fiber properties, we mount the fiber in such a way that the sensing part is unable to move, then mechanically compensating the strain variation effects.

We will now describe and explain the mounting steps of the test bench. In the Fig.20, we can see one of the two extremities of the fiber, the one that is not connected to the light and interrogating device. Note that, as we use the reflection properties of the fiber and as the fiber gets only one fiber Bragg Grating (then no interferences with a possible reflection in another segment of the fiber), we can let the fiber rolled at this extremity without any risks to falsify the measurements, the rest of the fiber is just here to connect this sensing segment to the interrogator. It is important to notice that if we were using a fiber with multiple sensing segments, we should focus on each one as they all contribute to the measurements. Then, on the Fig.21, we see the base of the first block that will keep the fiber in place, ensure that the fiber stay still. This base is a slab of metal with a groove that will be use as a guide to maintain the fiber straight. Then, as we can see in the Fig.22, once the base in place, we place the fiber in the guide and block it via the use of adhesive tape (this solution was chosen as it does not damage the fragile fiber, it is efficient enough and allow a simple change of fibers in case we want to test several fiber in a row). Finally, to complete this first block, we dispose another slab of metal on top and simply screw it to ensure that the fiber is well kept in place and do not slide, as in the Fig.23.

Figure 20: Fiber extremity

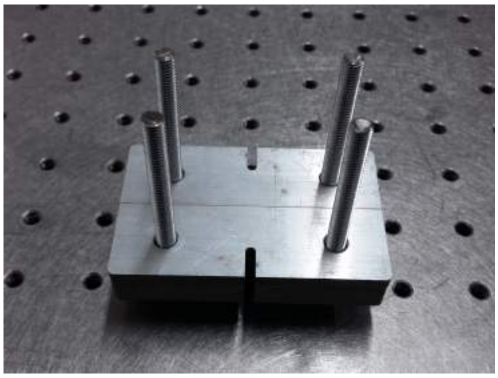

Figure 21: Base of the first blocking block

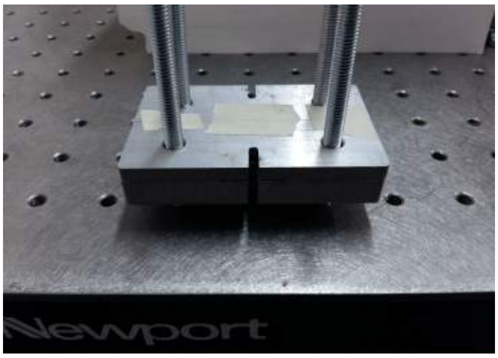

Figure 22: Fiber blocked with tape

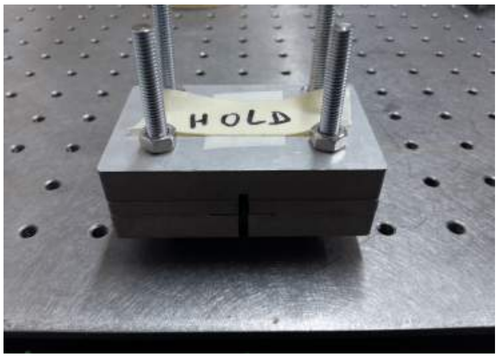

Figure 23: First blocking block top

Now one side of the fiber is blocked, we mount the sensing and heating block. First, we dispose the base. It is a metal slab that gets an extrusion were is clued the thermal sensor. The sensor is glued in a way that it is just sticking out of the surface of the slab, in order to be in direct contact of the fiber, thus providing us its actual temperature. In order to limit the pressure exerted on the fiber, we glued it with a thermal join (that is slightly soft) in order to absorb the pressure as much as possible, as we can see in Fig.24. Next, we dispose the fiber. To do so, we put, the fiber straight, fix it with adhesive tape (in order to insure that there will not be strain variation of the fiber in the sensing area) paying attention to perfectly place the fiber Bragg gratting (red segment of the fiber) on the sensor, as seen in Fig.25 and 26 in order to avoid to get hysteresis in our results due to the thermal inertia of the metal block (on Fig.46 in annexe we can see the hysteresis induced). Once the fiber is in place, we put another layer, a wood slab, that we can see in the figure number 27. This layer has two functions : the first one is, as the heating/cooling element is in our case a peltier cell, to isolate the two sides of the cell in order to have a cold and hot side well separated, thus allowing us to have a sharp difference of temperature and thus a faster change of temperature. The second function of the wood layer, as high as the peltier cell, is to avoid to put all the pressure that will be generated by the coming layer, on the peltier cell itself that will be disposed right on the fiber (this would possibly result in the cutting of the fiber). We can notice in the Fig.28 that the wood slab is cut in such a way that the peltier cell can not move and is maintained in place right above the thermal sensor and the sensing part of the fiber for optimal precision. Once this cell in place, we close the block via a metal slab and screw it by hand to avoid to generate excessive pressure. The final block is shown in the Fig.29. Here we can note two things : that the peltier cell is in contact with two metal blocks, otherwise it can not work and that the choice of wood to isolate thermicaly the two blocks of metal that the cell is touching is interesting as the thermal conductivity of the wood is more than ten times smaller than the one of metal (<1 W*m^{-1}*K^{-1} for the wood against one >10 W*m^{-1}*K^{-1} for the metal).

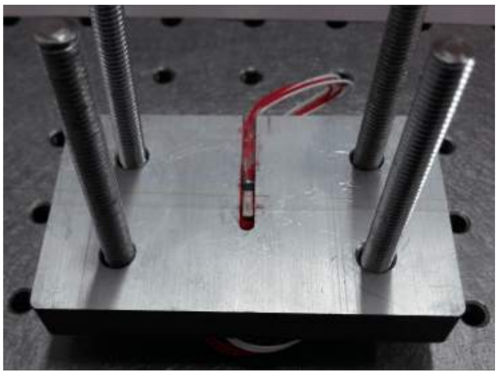

Figure 24: Base of the sensing block including the temperature sensor

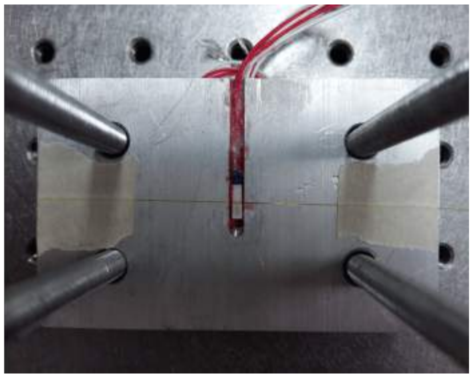

Figure 25: Fiber positioning and blocking, top view

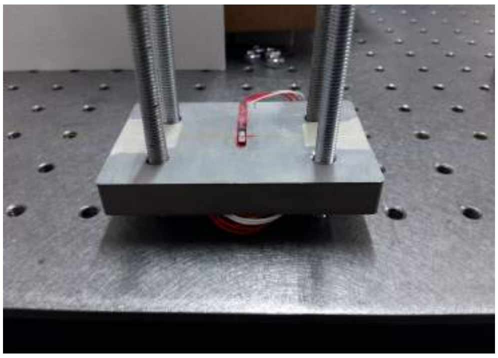

Figure 26: Fiber positioning and blocking

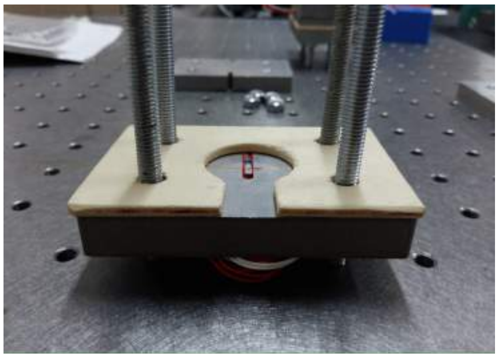

Figure 27: Wood slab

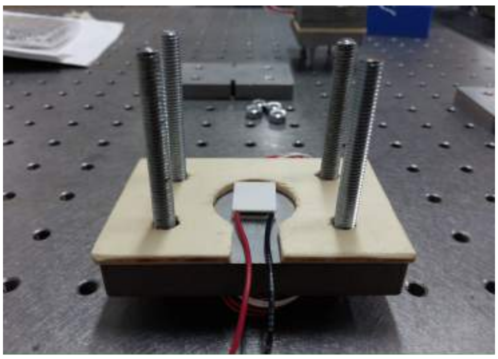

Figure 28: Peltier cell implementation

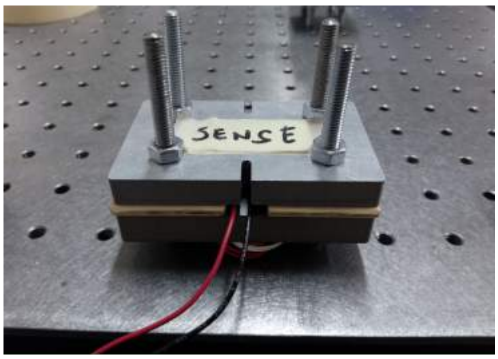

Figure 29: Top layer of the sensing block

Finally we block the fiber at the exit of the sensing block using a block identical to the first blocking one. Thus, we can see in Fig.30 the final aspect of the test bench before wiring the sensor and peltier cell to the controller, and once everything is connected in Fig.31.

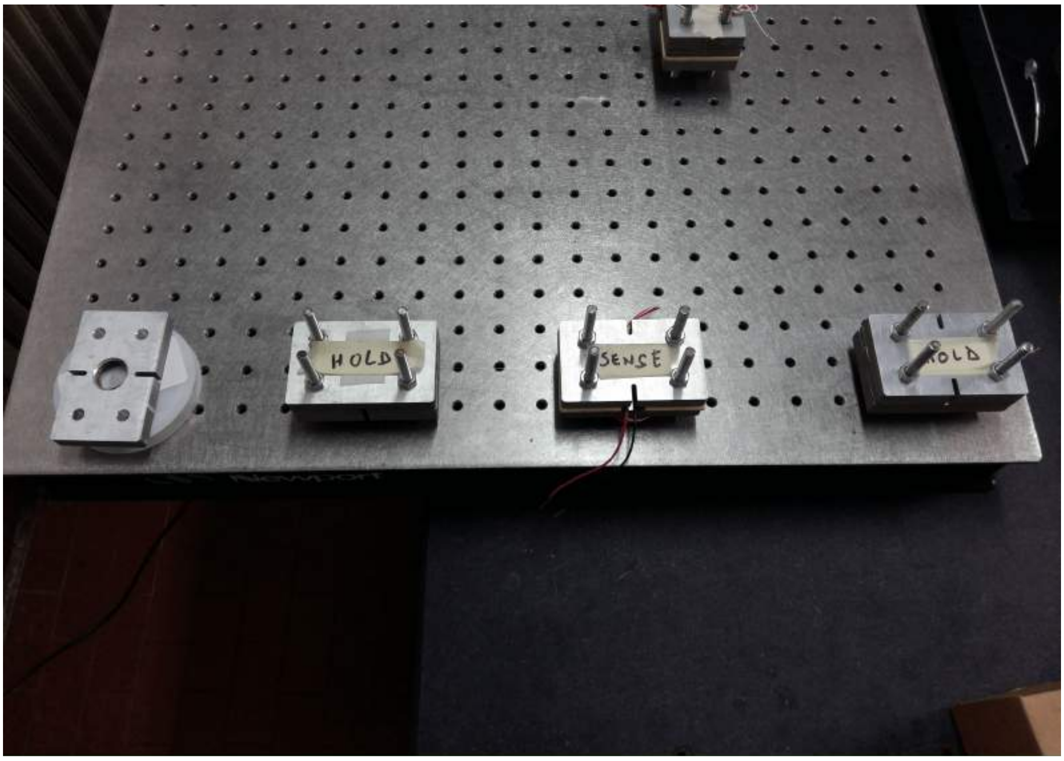

Figure 30: Test bench before wiring the controller

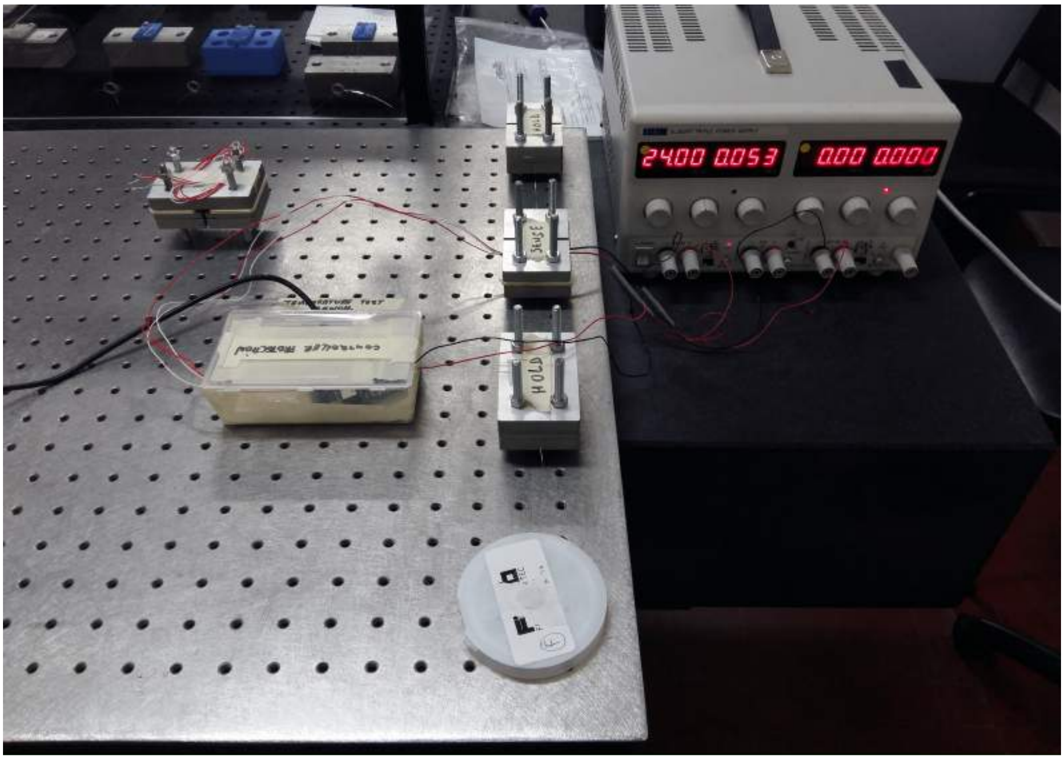

Figure 31: Test bench with the controller wired

As the controller has been delivered without protection, in order to avoid any issues, we put it in a plastic box cut on the sides, so that we can close the box without cutting the cables when we power on the controller (this way the user can not create a short circuit touching the device while it is turned on for example), as we can see in Fig.32.

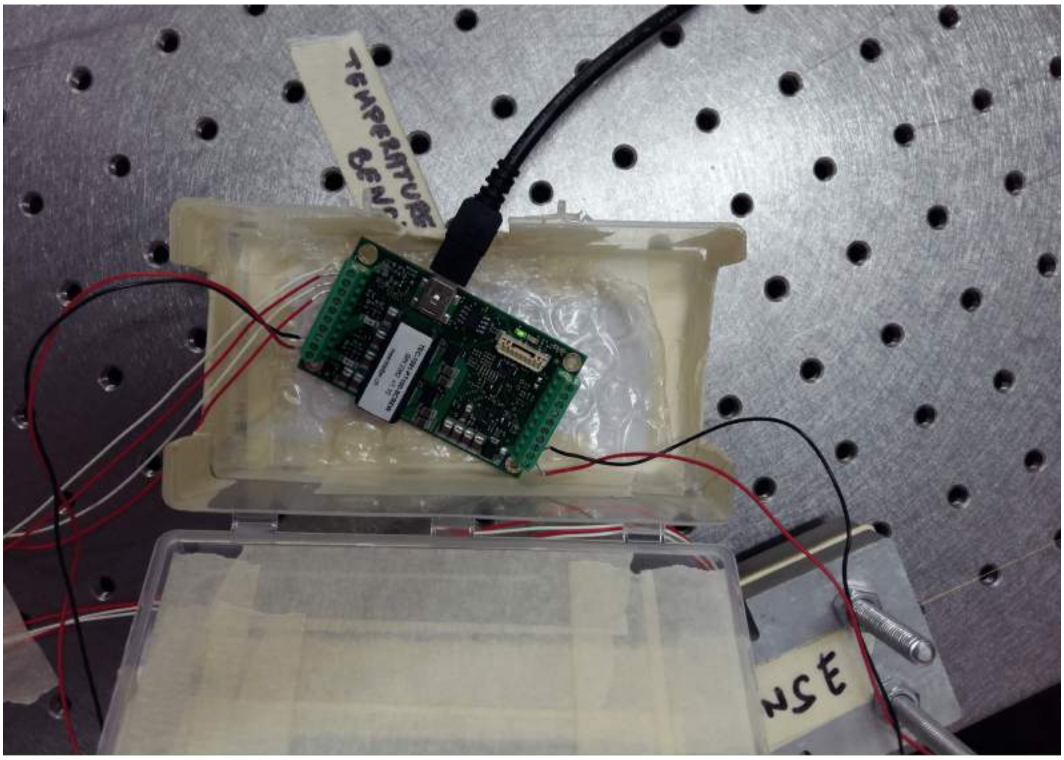

Figure 32: Controller in its protection box

The last step of the test bench mounting is the connection of the fiber to the interrogator. The interrogator we use, SmartScan from smart fibres, is an ultra-compact interrogator for measurement of FBG sensors equipped with a tunable laser. This tunable laser will be used as the light source. The fiber needs a special connector to be linked to the interrogator, shown in Fig.33, while in Fig.34 we can see the SmartScan interrogator connected to the rest of the system: the blue cable is the fiber that we want to characterize, the black cable is the alimentation and the white cable is an Ethernet cable, this is the one that will transmit the data from the interrogator to the pc where the data will be exploited via the software SmartSoft for SmartScan (v3.2).

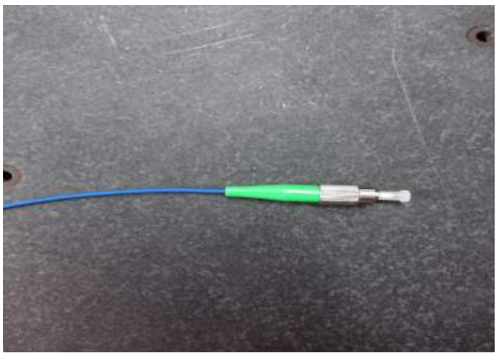

Figure 33: Extremity of the fiber connected to the interrogator

Figure 34: Fiber interrogator

IV - 3 Measurements

The protocol for the determination of the thermo-optical coefficient of the fiber is the following one : we set a desired temperature, then we wait that the system reaches a steady state in term of the temperature and read the wavelength value of the reflected wave. Applying this protocol on a given range of temperature, we obtain a curve from which we can extract the thermo-optical coefficient of the fiber, as it is the coefficient of the obtained curve itself.

For our tests, as we do not know precisely the range of temperature of the fiber we use and as the peltier gets a maximum difference of 74 degrees between both sides with the hot side at maximum 90 ˚C (note that the laboratory is at a controlled temperature of 23 ˚C), we will work is relatively small ranges of temperature, starting from 14 degres to maximum 40 degres (we will pay attention not to go over) in order to work in a safe range for all the components of the system. In order to ensure that our test bench is working properly, that we heat or cool the fiber, we carry each serie of measurement in two times : first we heat the fiber, with a given temperature increment, and then we cool it with the same conditions as for the heating. The reading of the wavelength is done via the software SmartSoft as we can see on the Fig.35 and the value of the temperature via TEC Service Sofware as we can see on the Fig.36 and 37 (when the temperature is indicated in orange, it means that we are not yet is steady state while when it is green, it means that we have reached the steady state). For more details about the setting of the TEC Service Software, see Fig.49, Fig.50 and Fig.51 in annexe.

It is important to mention that to get a response as good as possible from the system, we avoid to curve the fiber will small radius of curvature between the sensing part of the fiber and the interrogator, as it would decrease the intensity of the reflected wavelength (we can see the difference between a fiber placed avoiding small radius of curvature and one that is not avoiding them via Fig.47 and Fig.48).

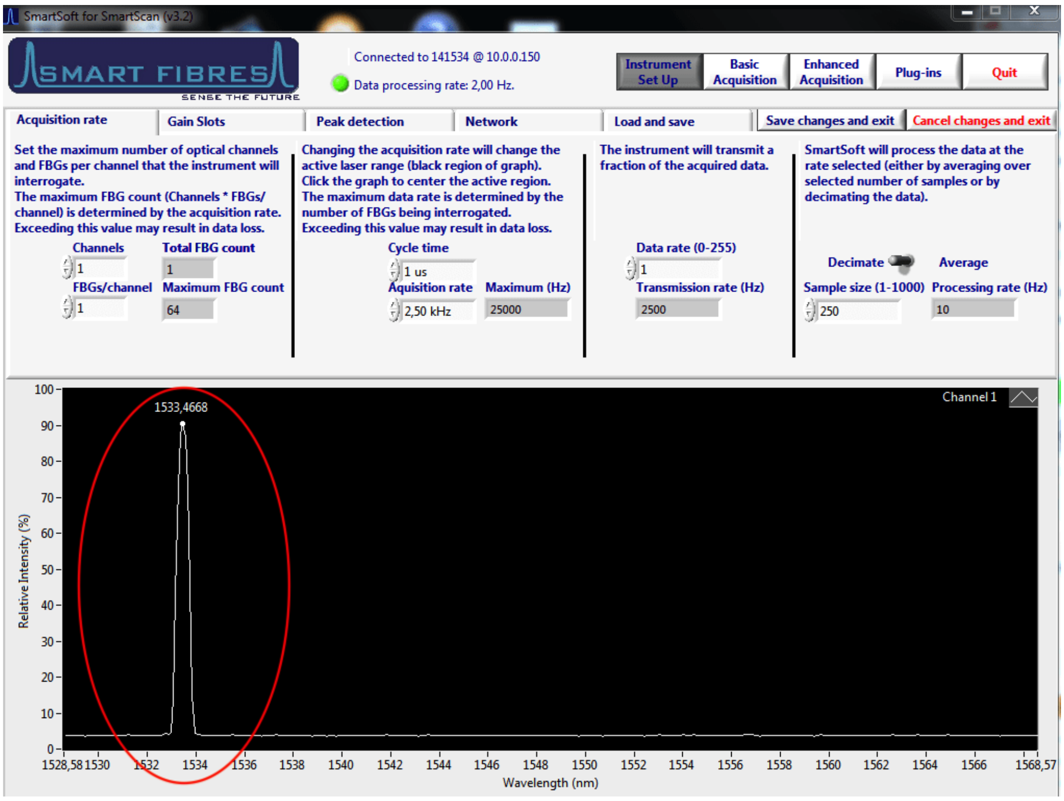

Figure 35: Wavelength display on SmartSoft

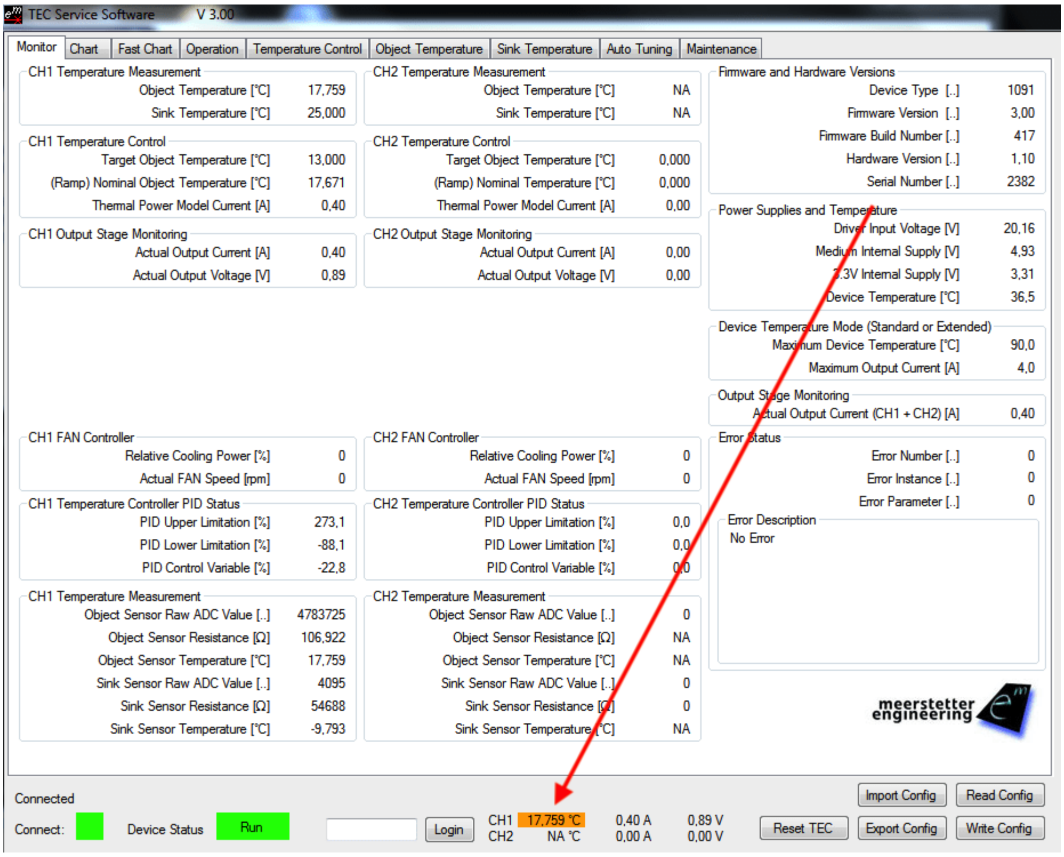

Figure 36: TEC Service Software before steady state

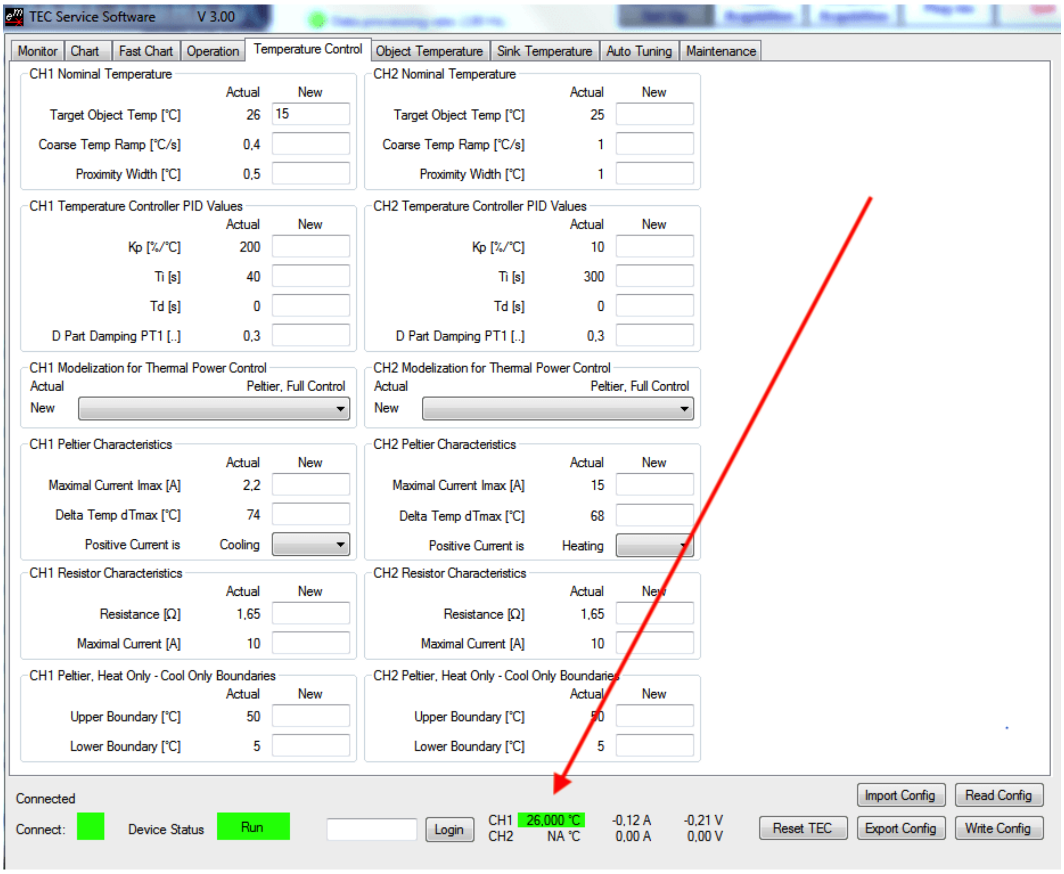

Figure 37: TEC Service Software at steady state

For our first test, we use a 5 degrees increment and we wait 2 minutes before taking the wavelength (even if we reach a steady state after some seconds) to be sure that the thermal inertia of the sensing block (due to the thermal inertia of the metal) does not influence our measurements.The results of this first test are displayed in the table 1, and then we obtain the experimental curves shown in Fig.38. Fig.39 displays the linear regressions of the two experimental curves (for heating and cooling).

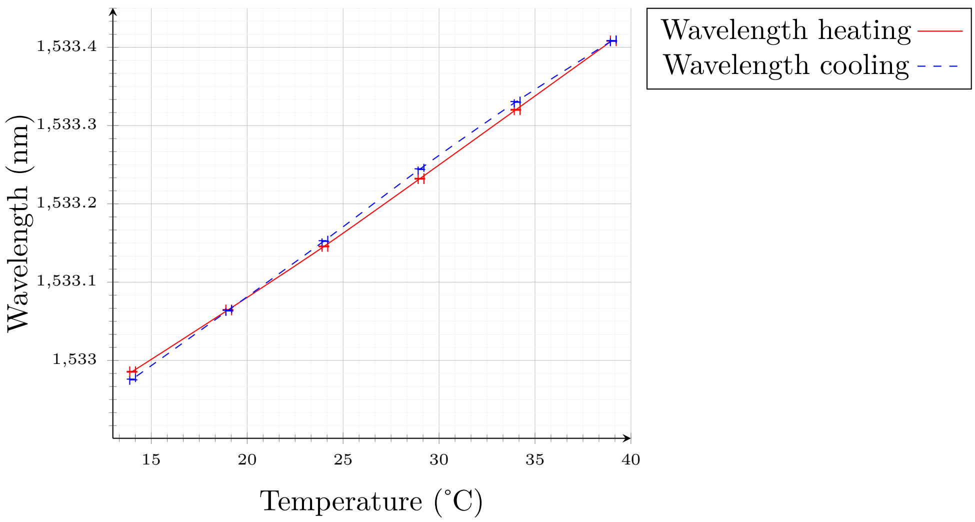

Figure 38: First test experimental curves

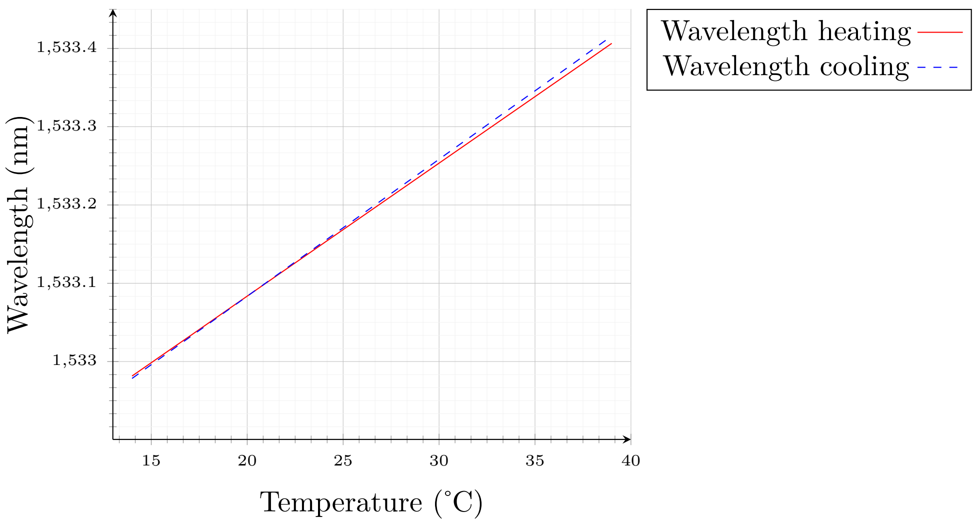

Figure 39: Linear regressions for the first test

The linear regressions of the two experimental curves, for heating and cooling, respectively get the following equations :

$$y = 0.0170x + 1,532.743 \tag{14}$$

$$y = 0.0175x + 1,532.733 \tag{15}$$

For equation 14 and equation 15 the linear correlation coefficients are respectively $R^2 = 0.9995$ and $R^2 = 0.9994$.

Then, in the second test we use an increment of 3 degrees and we wait 50 seconds to reach a steady state. The waiting time is reduced compare to the previous test as the temperature increment is reduced. The results of this test are displayed in the table 2, and then we obtain the experimental curves shown in Fig.40. Fig.41 displays the linear regressions of the two experimental curves (for heating and cooling).

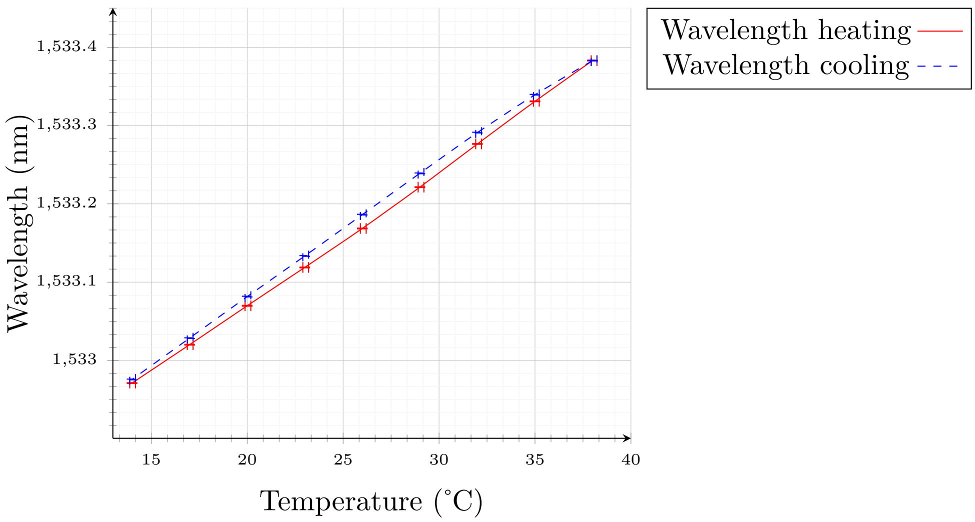

Figure 40: Second test experimental curves

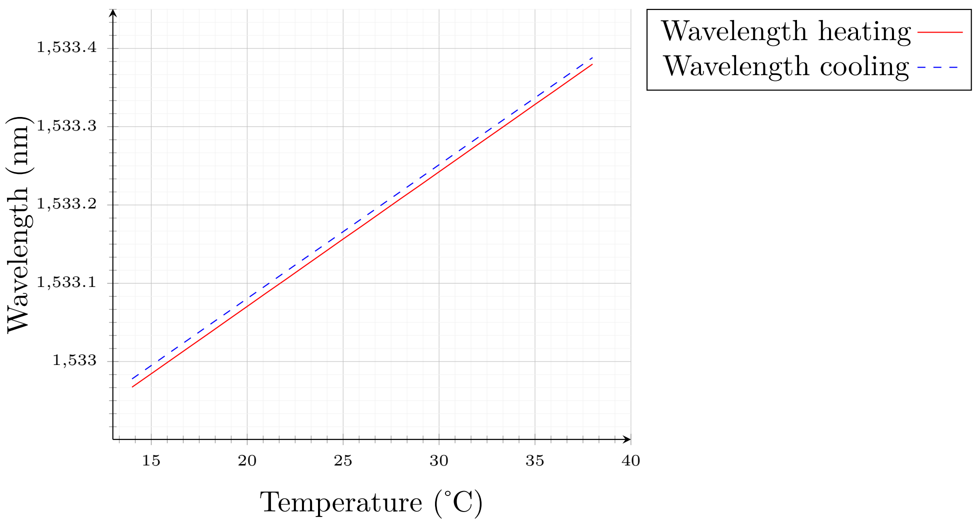

Figure 41: Linear regressions for the second test

The linear regressions of the two experimental curves, for heating and cooling, respectively get the following equations :

$$y = 0.0172x + 1,532.726 \tag{16}$$

$$y = 0.0171x + 1,532.738 \tag{17}$$

For the equation number 16 and the equation number 17 the linear correlation coefficients are $R^2 = 0.9995$ and $R^2 = 0.9994$.

Next, for our third test we use a 2 degrees increment and we wait 30 seconds to reach a steady state. Once again the waiting time is reduced as the temperature increment is reduced compare to the second test. The results of this test are displayed in the table 3, and then we obtain the experimental curves shown in Fig.42. Fig.43 displays the linear regressions of the two experimental curves (for heating and cooling).

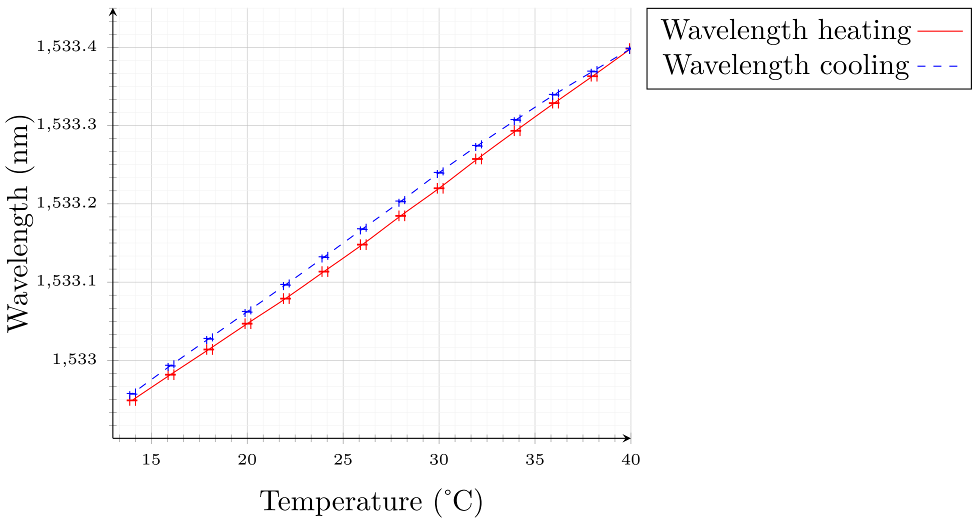

Figure 42: Third test experimental curves

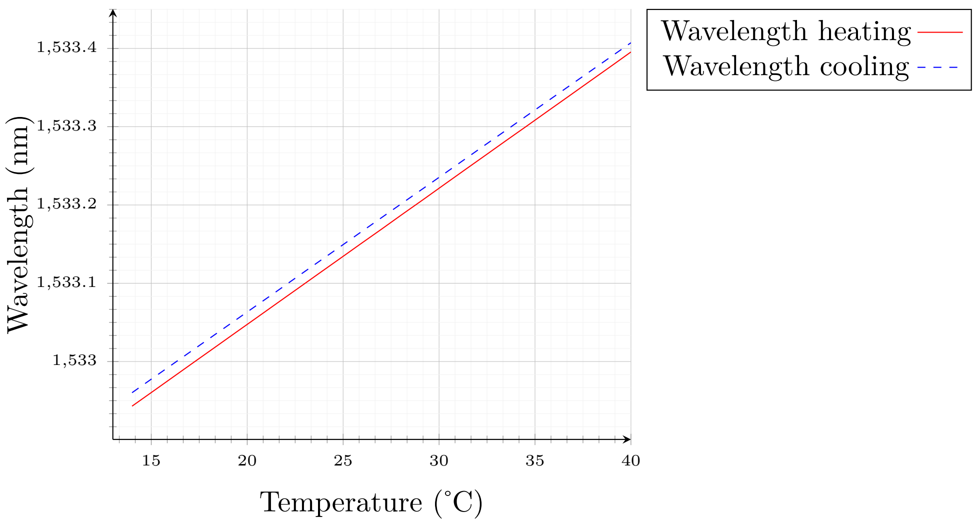

Figure 43: Linear regressions for the third test

The linear regressions of the two experimental curves, for heating and cooling, respectively get the following equations :

$$y = 0.0174x + 1,532.699 \tag{18}$$

$$y = 0.0172x + 1,532.719 \tag{19}$$

For the equation 18 the linear correlation coefficient is $R^2 = 0.9996$ and for the equation 19 the linear correlation coefficient is $R^2 = 0.9994$.

In the fourth test we use an increment of 5 degrees and we wait 1 minute to reach a steady state. In this test, we divide the waiting time by two compared to the first test that was also with a 5 degrees increment but it is enough to avoid any effects due to the thermal inertia of the block. The results of this final test are displayed in the table 4, and then we obtain the experimental curves shown in Fig.44. Fig.45 displays the linear regressions of the two experimental curves (for heating and cooling).

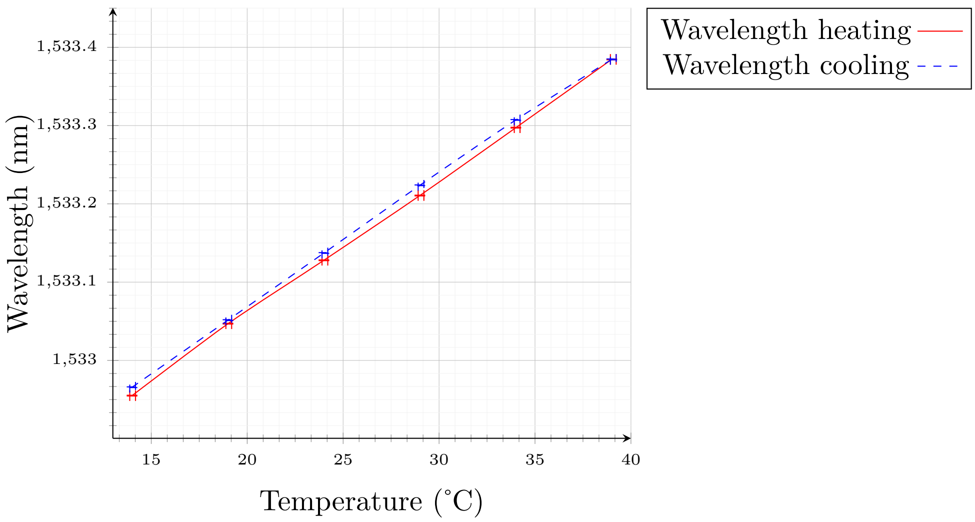

Figure 44: Fourth test experimental curves

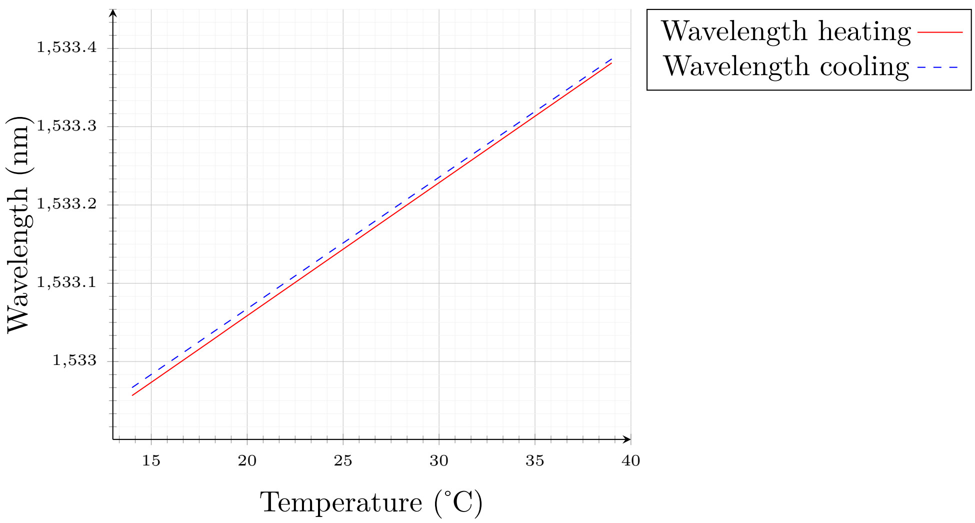

Figure 45: Linear regressions for the fourth test

The linear regressions of the two experimental curves, for heating and cooling, respectively get the following equations :

$$y = 0.0170x + 1,532.718 \tag{20}$$

$$y = 0.0168x + 1,532.731 \tag{21}$$

For the equation 20 and for the equation number 21 the linear correlation coefficients are respectively $R^2 = 0.9998$ and $R^2 = 0.9997$.

The experimentally obtained fiber coefficients are summed up in tab 5.

The formula to obtain the incertitude of a result calculated as the average of a set of data is the following one (with k a factor and n the number of measurements):

$$U = k.\sqrt{\frac{1}{n}.\frac{1}{n-1}.\sum_{i=1}^{n}(x_i - \bar{x})^2} \tag{22}$$

Finally, averaging the previously obtained coefficients and applying the equation 22 (we chose the factor k in such a way to get a 95% confidence level), we obtain the desired value, the thermo-optical coefficient of our fiber, that is :

$$thermal\ coef. \ = \ 1.72\ .\ 10^{-11}\ \pm\ 2\ .\ 10^{-13}\ m.^{\circ}C^{-1}$$

IV - 4 Analysis of the results

The first thing we can say about our results, is that they are all in the order of magnitude of the FBG sensor thermo-optical coefficient, 10^{-11} $m.^{\circ}C^{-1}$. But, despite being in the correct order of magnitude, our values seems to be slightly over the common values for FBG sensors, as it is common to find around $0.010.10^{-11}$ m.$^{\circ}$C^{-1} [14, 18]. This can be due to the pressure applied on the sensing segment (pressure induced by the peltier, the top slab of the sensing block and the pressure induced by the screwing) and the induced tension of the fiber due to its mounting that could prevent the fiber to behave properly in our tests. It is also important to mention the fact that we did not get provided the data of the fiber, so we did not know the material it is made of neither the coefficient that the supplier found. Thus, our results could be correct but we can not compare them to the theoretical value of the coefficient for the fiber material neither to the value that the supplier could have provided.

We can nonetheless say that we have tried to decrease the tension of the fiber implementing it straight without adhesive tape, curved with and without adhesive, in order to see if we could obtain different results but we have not obtained satisfying results.

In order to improve the quality of the test bench it would also be necessary to improve the quality of the wiring as electromagnetic noise can affect our measurement as we are using basic wires.

V Conclusion

The project was to create a test bench to determine the thermo-optical coefficient of a sensing optical fiber, the sensing being done via fiber Bragg Grating (FBG).

To this aim we created a regulated test bench using a feedback control loop for an optimal control of the temperature using a controller which aim was to drive a peltier cell according to the state of the system, that was provided via a thermal sensor, to keep the fiber at the desired temperature we set originally. After testing the fiber on a given range of temperature multiple times with different temperature increments, we have obtained an experimental set of measurements from which we have extracted the experimental thermo-optical coefficient of the fiber that is $1.72 \,.\, 10^{-11} \pm 2 \,.\, 10^{-13}\ m.^{\circ}C^{-1}$. This value is a satisfying result as it is in the order of magnitude of FBG thermo-optical coefficient, $10^{-11}\ m.^{\circ}C^{-1}$.

Nevertheless, the quality of our measurements was limited as this kind of fiber is also sensitive to strain and we did not know if the fiber was undergoing strain induced by the manual positioning. Furthermore the fiber, that is also pressure sensitive, was undergoing pressure, generated by the presence of the slab of metal on top of the sensing block or/and by the screwing, that possibly affected the behavior of the FBG.

Thus, as the Politecnico di Torino could be interested to produce its own sensing fibers in a near futur, printing the Bragg Grating inside the core of the fibers, the current precision should be increased so that the test bench could be used for the thermo-optical coefficient determination and certification of the fibers produced. It could be done with the implementation of a device that ensures to apply the same tension to every fiber tested and to position the sensing segment in such a way that it is not subject to pressure induced by another component (the difficulty being to find a compromise between not putting pressure and the fiber and hold it enough so that no strain variation can take place). It is also important to mention that our results will be used by people who work on the thermal compensation to study strain variation via FBG sensing.

To conclude, I would say that this thesis was truly interesting for me as I discovered an efficient sensing technology with plenty of possible application domains (from structure health monitoring to aeronautics for example). My only regret is that the late access to the facilities (a month before the end of the thesis) and the time lost due to problems encountered on some components of the test bench once getting the access to the laboratory, prevented me from going further in the development of the test bench to increase the quality of the results trying new solutions.

VI References

[1] Raman Kashyap, “Fiber Bragg Gratings”, Elsevier, 2009

[2] Yun-Jiang Rao, “In-fiber Bragg Grating sensors”, Measurement Science and Technology, 2009

[3] Pierre Lecoy, “Les fibres optiques en capteurs et en instrumentation”, 13, La Revue 3E.I (SEE), 2016,

[4] Noritomo Hirayama and Yasukazu Sano, “Fiber Bragg grating temperature sensor for practical use”, Elsevier, 2000

[5] Stephen J. Mihailov, “Fiber Bragg Grating Sensors for Harsh Environments”, 1898-1918, 12, Sensors, 2012

[6] Mathieu Gagné, “Fabrication et applications des réseaux de Bragg ultra-longs”, PhD thesi, Montreal University, 2015

[7] National Instruments, “Principes fondamentaux des capteurs à fibre optique FBG”, http://www.ni.com/white-paper/11821/fr/, 2012

[8] Sanjeev Dewra, Vikas and Amit Grover, “Fabrication and Applications of Fiber Bragg Grating- A Review”, Adv. Eng. Tec. Appl. 4, , No. 2, 15-25, 2015

[9] Kenneth O. Hill and Gerald Meltz, Member, IEEE, “Fiber Bragg Grating Technology Fundamentals and Overview”, Journal of lightwave technology, vol.15, No. 8, 1997

[10] Kenneth O. Hill, B. Malo, F. Bilodeau, D. C. Johnson, and J. Albert, “Bragg gratings fabricated in monomode photosensitive optical fiber by UV exposure through a phase mask”, Applied Physics Letters 62, 1035, 1993

[11] R. Paschotta, “Fiber Bragg Gratings”, Encyclopedia of Laser Physics and Technology, 2008

[12] Victor Giurgiutiu, “Structural Health Monitoring of Aerospace Composites”, 249-296, 7, Elsevier, 2016

[13] K. O. Hill, B. Malo, F. Bilodeau, D. C. Johnson, and J. Albert, “Bragg gratings fabricated in monomode photosensitive optical fiber by UV exposure through a phase mask”, Appl. Phys. Lett., Vol. 62, No. 10, 8 March 1993

[14] Stephen J. Mihailov, “Fiber Bragg Grating Sensors for Harsh Environments”, 1898-1918, 2012

[15] Ebrahim Oromiehie, B. Gangadhara Prusty, Paul Compston Ginu Rajan, “In-situ simultaneous measurement of strain and temperature in automated fiber placement (AFP)

using optical fiber Bragg grating (FBG) sensors", Advanced Manufacturing: Polymer Composites Science, 3:2, 52-61, 2017

[16] O Frazao and al, "Simultaneous measurement of strain and temperature using fibre Bragg gratings in a twisted configuration", J. Opt. A: Pure Appl. Opt. 7 427, 2005

[17] Yun-Jiang Rao, og In-fibre Bragg grating sensors", Meas. Sci. Technol. 8 355, 1997

[18] Noritomo Hirayama and Yasukazu Sano, og Fiber Bragg grating temperature sensor for practical use", Elsevier, 2000

[19] Nobuhira Tanaka and al, og Temperature-compensated strain measurement using fiber Bragg grating sensors embedded in composite laminates", Smart Mater. Struct. 12 940, 2003

[20] Daniele Tosi, og Review of Chirped Fiber Bragg Grating (CFBG) Fiber-Optic Sensors and Their Applications", Sensors, 18, 2147, 2018

[21] Tong Zhao, Qi Wang and He Huang, og Characteristics and applications of tilted fiber Bragg gratings", Journal of optoelectronics and advanced materials Vol. 12, No. 12, p. 2343 - 2354, December 2010

[22] Ebrahim Oromiehie, Ginu Rajan and B Gangadhara Prusty, og Thermal sensitivity and relaxation of carbon fibre-foam sandwich composites with fibre optic sensors", Journal of Sandwich Structures and Materials, Vol. 18(5) 652–664, 2016

[23] I. Ashry, A. Elrashidi, A. Mahros, M. Alhaddad, and K. Elleithy, og Investigating the Performance of Apodized Fiber Bragg Gratings for Sensing Applications", 2014

[24] Xiaoyi Dong, Hao Zhang, Bo Liu, and Yinping Miao, og Tilted Fiber Bragg Gratings: Principle and Sensing Applications", Photonic Sensors Vol. 1, No. 1: 6-30, 2011

[25] Alejandro Martinez-Rios, David Monzon-Hernandez, Ismael Torres-Gomez and Guillermo Salceda-Delgado, og Long Period Fibre Gratings", Fiber Optic Sensors, 275-294, 2012

[26] Optromix, "Phase-shifted fiber Bragg gratings (πFBGs)", https://fibergratings.com/wp/uncatego
shifted-fiber-bragg-gratings-fbgs/, 2016

[27] Govind P. Agrawal and Stojan Radic, "Phased-Shifted Fiber Bragg Gratings and their Application for Wavelegnth Demultiplexing", IEEE Photonics technology letters, Vol. 6, No. 8, 1994

[28] Patrik Rugeland, "Tunable Phase-shifted fiber Bragg gratings and its applications in the microwave region", Master of Science Thesis, 2009

[29] Ebrahim Al-Fakih, Noor Azuan Abu Osman and Faisal Rafiq Mahamd Adikan, "The Use of Fiber Bragg Grating Sensors in Biomechanics and Rehabilitation Applications: The State-of-the-Art and Ongoing Research Topics", Sensors, 12(10), 12890-12926, 2012

[30] Pierrick Vulliez, "FIBER-OPTIC SENSING: Distributed fiber-optic sensing solves real-world problems", https://www.laserfocusworld.com/articles/2013/01/fiber-optic-sensing-distributed-fiber-optic-sensing-solves-real-world-problems.html, 2013

VII List of tables

Wavelength (nm)	Temperature (°C)
1,532.9851 ± 0.0005	14.00 ± 0.15 + 0,03
1,533.0640 ± 0.0005	19.00 ± 0.15 + 0,04
1,533.1451 ± 0.0005	24.00 ± 0.15 + 0,05
1,533.2317 ± 0.0005	29.00 ± 0.15 + 0,06
1,533.3197 ± 0.0005	34.00 ± 0.15 + 0,07
1,533.4078 ± 0.0005	39.00 ± 0.15 + 0,08
1,533.3297 ± 0.0005	34.00 ± 0.15 + 0,07
1,533.2439 ± 0.0005	29.00 ± 0.15 + 0,06
1,533.1520 ± 0.0005	24.00 ± 0.15 + 0,05
1,533.0632 ± 0.0005	19.00 ± 0.15 + 0,04
1,532.9752 ± 0.0005	14.00 ± 0.15 + 0,03

Table 1: First test results

Wavelength (nm)	Temperature (°C)
1,532.9706 ± 0.0005	14.00 ± 0.15 + 0,03
1,533.0196 ± 0.0005	17.00 ± 0.15 + 0,03
1,533.0693 ± 0.0005	20.00 ± 0.15 + 0,04
1,533.1183 ± 0.0005	23.00 ± 0.15 + 0,05
1,533.1681 ± 0.0005	26.00 ± 0.15 + 0,05
1,533.2209 ± 0.0005	29.00 ± 0.15 + 0,06
1,533.2761 ± 0.0005	32.00 ± 0.15 + 0,06
1,533.3305 ± 0.0005	35.00 ± 0.15 + 0,07
1,533.3825 ± 0.0005	38.00 ± 0.15 + 0,08
1,533.3389 ± 0.0005	35.00 ± 0.15 + 0,07
1,533.2906 ± 0.0005	32.00 ± 0.15 + 0,06
1,533.2386 ± 0.0005	29.00 ± 0.15 + 0,06
1,533.1857 ± 0.0005	26.00 ± 0.15 + 0,05
1,533.1329 ± 0.0005	23.00 ± 0.15 + 0,05
1,533.0810 ± 0.0005	20.00 ± 0.15 + 0,04
1,533.0280 ± 0.0005	17.00 ± 0.15 + 0,03
1,532.9752 ± 0.0005	14.00 ± 0.15 + 0,03

Table 2: Second test results

Wavelength (nm)	Temperature (°C)
1,532.9484 ± 0.0005	14.00 ± 0.15 + 0,03
1,532.9813 ± 0.0005	16.00 ± 0.15 + 0,03
1,533.0135 ± 0.0005	18.00 ± 0.15 + 0,04
1,533.0464 ± 0.0005	20.00 ± 0.15 + 0,04
1,533.0785 ± 0.0005	22.00 ± 0.15 + 0,04
1,533.1130 ± 0.0005	24.00 ± 0.15 + 0,05
1,533.1474 ± 0.0005	26.00 ± 0.15 + 0,05
1,533.1842 ± 0.0005	28.00 ± 0.15 + 0,06
1,533.2194 ± 0.0005	30.00 ± 0.15 + 0,06
1,533.2569 ± 0.0005	32.00 ± 0.15 + 0,06
1,533.2929 ± 0.0005	34.00 ± 0.15 + 0,07
1,533.3282 ± 0.0005	36.00 ± 0.15 + 0,07
1,533.3626 ± 0.0005	38.00 ± 0.15 + 0,08
1,533.3979 ± 0.0005	40.00 ± 0.15 + 0,08
1,533.3687 ± 0.0005	38.00 ± 0.15 + 0,08
1,533.3389 ± 0.0005	36.00 ± 0.15 + 0,07
1,533.3067 ± 0.0005	34.00 ± 0.15 + 0,07
1,533.2738 ± 0.0005	32.00 ± 0.15 + 0,06
1,533.2393 ± 0.0005	30.00 ± 0.15 + 0,06
1,533.2026 ± 0.0005	28.00 ± 0.15 + 0,06
1,533.1673 ± 0.0005	26.00 ± 0.15 + 0,05
1,533.1314 ± 0.0005	24.00 ± 0.15 + 0,05
1,533.0961 ± 0.0005	22.00 ± 0.15 + 0,04
1,533.0617 ± 0.0005	20.00 ± 0.15 + 0,04
1,533.0272 ± 0.0005	18.00 ± 0.15 + 0,04
1,532.9928 ± 0.0005	16.00 ± 0.15 + 0,03
1,532.9568 ± 0.0005	14.00 ± 0.15 + 0,03

Table 3: Third test results

Wavelength (nm)	Temperature (°C)
1,532.9545 ± 0.0005	14.00 ± 0.15 + 0,03
1,533.0464 ± 0.0005	19.00 ± 0.15 + 0,04
1,533.1275 ± 0.0005	24.00 ± 0.15 + 0,05
1,533.2102 ± 0.0005	29.00 ± 0.15 + 0,06
1,533.2968 ± 0.0005	34.00 ± 0.15 + 0,07
1,533.3841 ± 0.0005	39.00 ± 0.15 + 0,08
1,533.3067 ± 0.0005	34.00 ± 0.15 + 0,07
1,533.2232 ± 0.0005	29.00 ± 0.15 + 0,06
1,533.1367 ± 0.0005	24.00 ± 0.15 + 0,05
1,533.0510 ± 0.0005	19.00 ± 0.15 + 0,04
1,532.9652 ± 0.0005	14.00 ± 0.15 + 0,03

Table 4: Fourth test results

Fiber thermo-optical coefficient (nm*$^{\circ}C^{-1}$)
0.0170 ± 0.0002
0.0175 ± 0.0002
0.0172 ± 0.0003
0.0171 ± 0.0003
0.0174 ± 0.0002
0.0172 ± 0.0002
0.0170 ± 0.0002
0.0168 ± 0.0002

Table 5: Experimentally obtained fiber coefficients

VIII Annexe

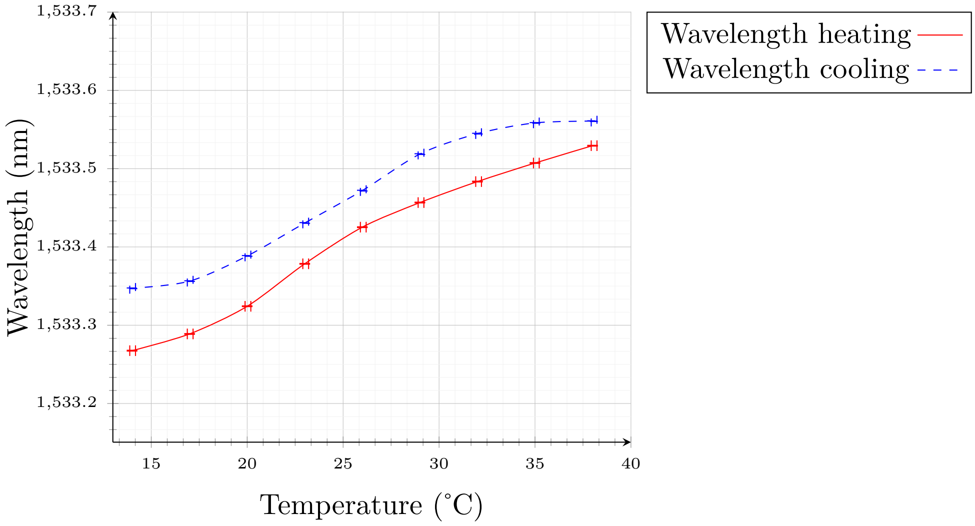

Figure 46: Hysteresis induced by the thermal inertia of the metal block

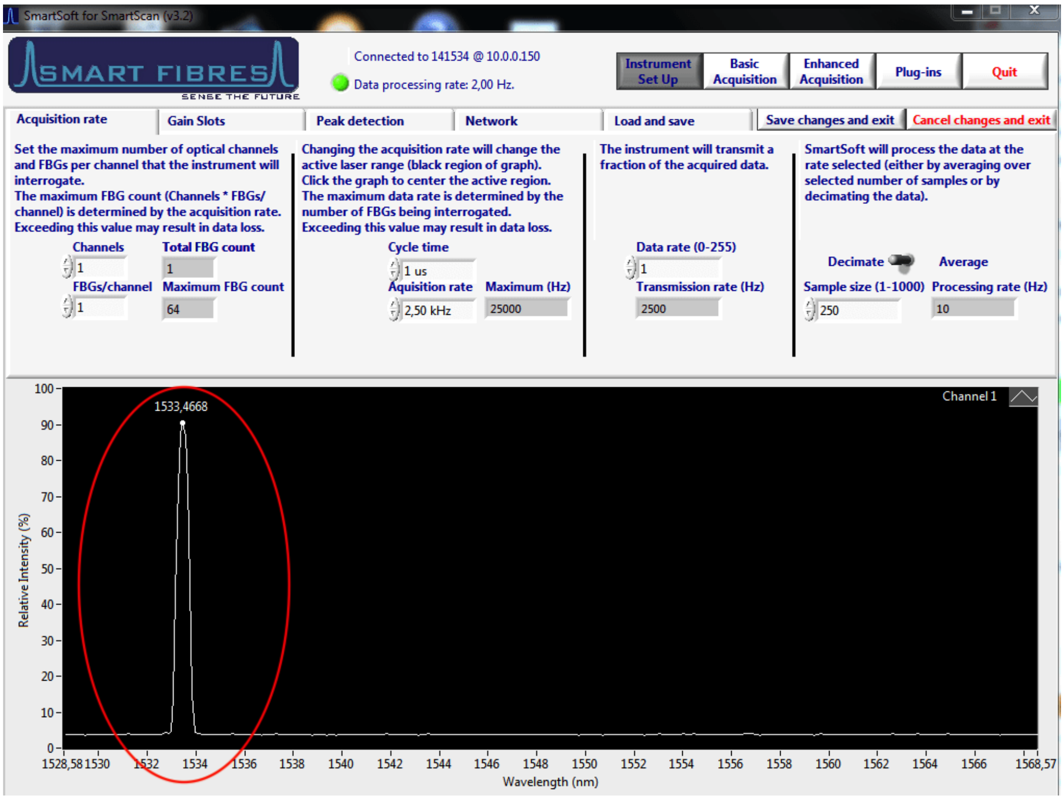

Figure 47: Response with curved fiber avoiding small radius of curvature

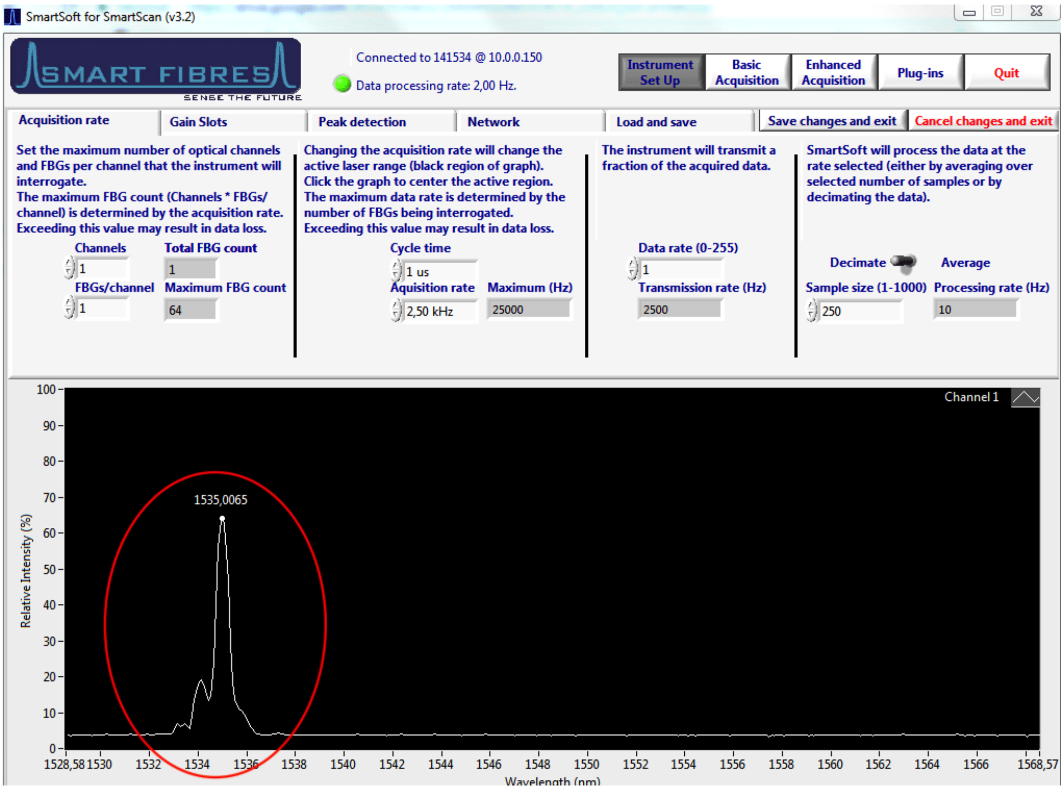

Figure 48: Response with curved fiber with small radius of curvature

We can see than the relative intensity of the reflected signal is lower than when we avoid small radius of curvature and another wavelength is slightly reflected.

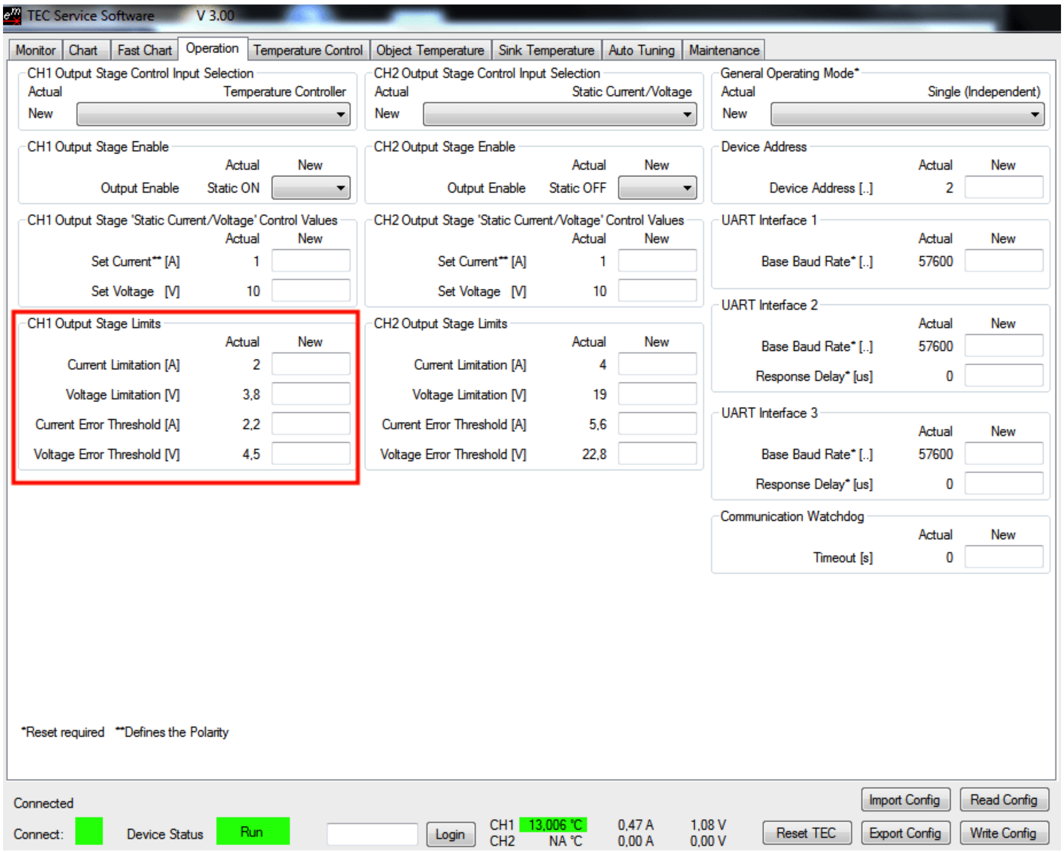

Figure 49: Parameters set to protect the Peltier cell (1)

The TEC Service Software V 3.00 allows us to set the current limitation, that we put 0,2A lower than the maximum current of the Peltier cell we used in order to protect the Peltier avoiding to push it to its limit. We set the voltage limitation to the maximum of the cell, the current error threshold at the maximum current of the Peltier cell and the voltage error threshold 20 percent higher than the maximum voltage of the cell as indicated in the setup guide of the software (the current error threshold should also be 20 percent higher than the maximum current value but we choose to put it at the maximum current value to protect the system, once more to avoid to push it to its limits).

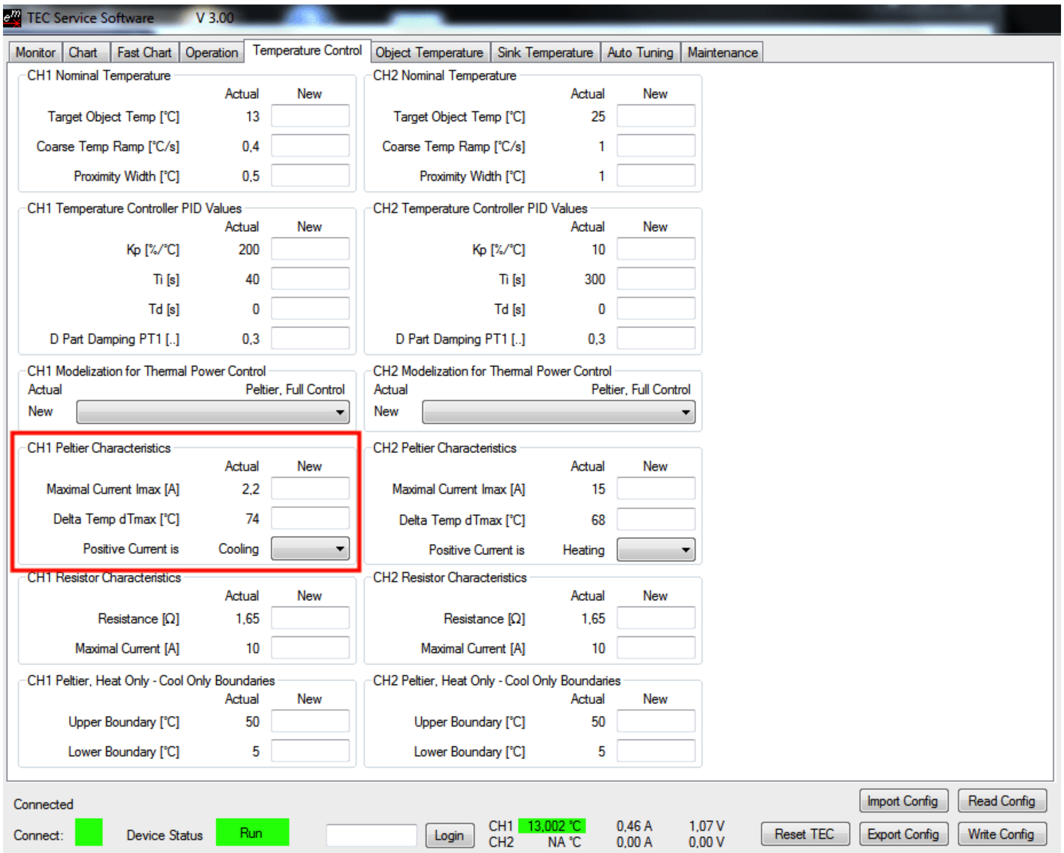

Figure 50: Parameters set to protect the Peltier cell (2)

TEC Service Software V 3.00 also allows us to set the maximum delta of temperature between the two sides of the Peltier cell, we put the value that is provided in the datasheet of the cell.

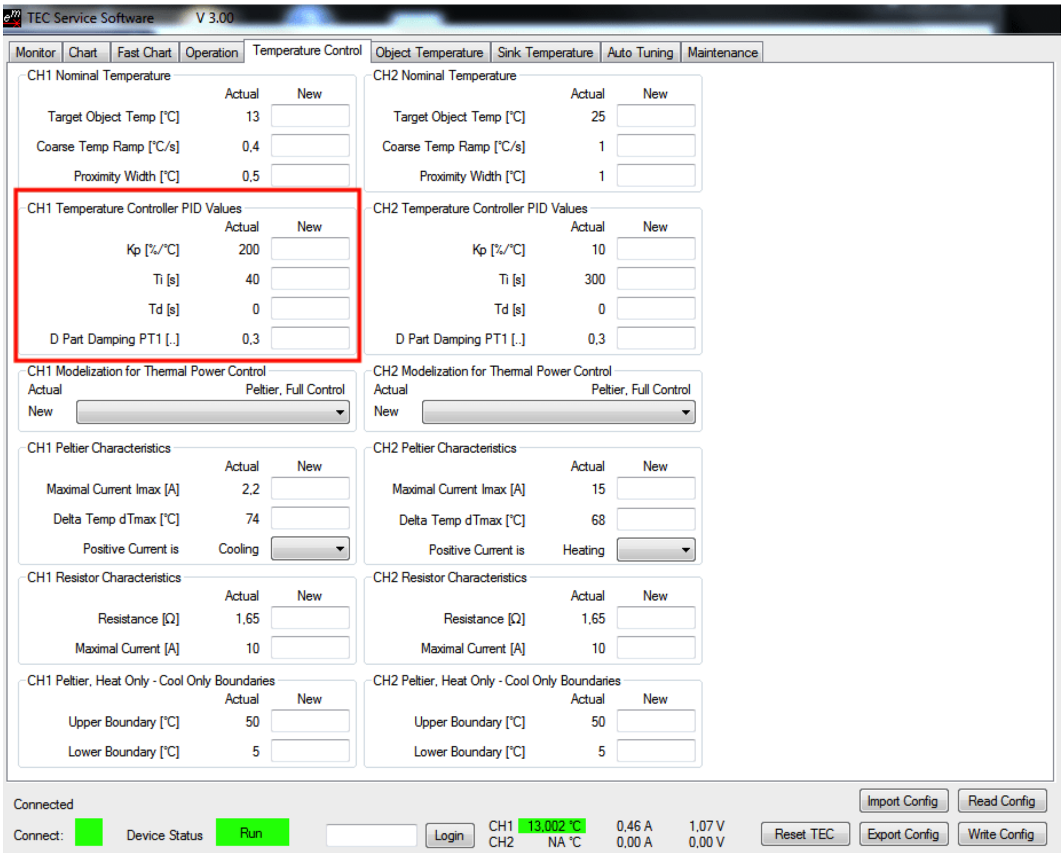

Figure 51: PID parameters set to obtain a fast and accurate system

To obtain this parameters, we first ran the software with standard coefficients. Then, the auto tuning of the system proposed us new values to optimize our system. We used this new values of the parameters and, according to the answer of the system after this optimization, we manually adjusted the parameters to get a fast and precise system.

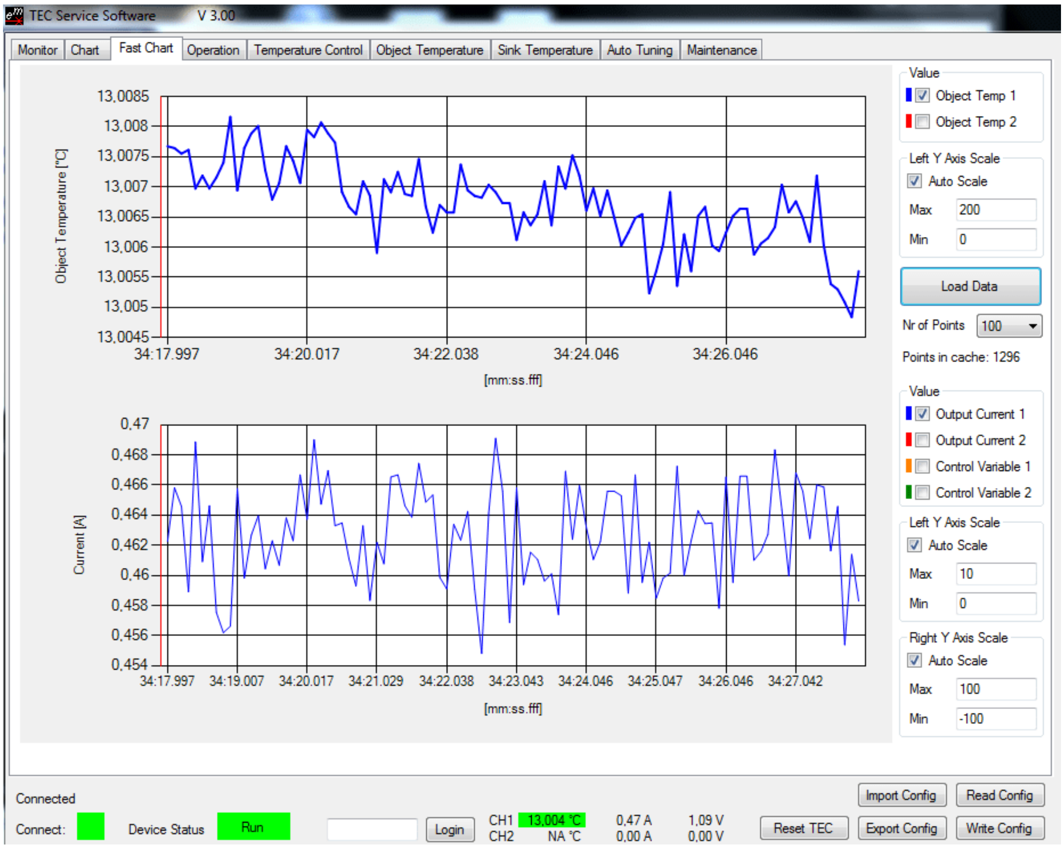

Figure 52: Real time display of temperature and current evolution